Aus der Klinik und Poliklinik für Radiologie
der Ludwig-Maximilians-Universität München
Direktor: Prof. Dr. med. Jens Ricke

Die Rolle der dynamischen kontrastverstärkten Magnetresonanztomographie in der Evaluation von neuroendokrinen Lebermetastasen

Dissertation
zum Erwerb des Doktorgrades der Humanmedizin
an der Medizinischen Fakultät der
Ludwig-Maximilians-Universität München

vorgelegt von
Marco Armbruster
aus Stuttgart
2021

Mit Genehmigung der Medizinischen Fakultät

der Universität München

Berichterstatter:	Prof. Dr. med. Wieland Sommer
Mitberichterstatter:	Prof. Dr. Christoph Auernhammer
	PD Dr. Harun Ilhan
Mitbetreuung durch den promovierten Mitarbeiter:	Prof. Dr. med. Christoph Zech
Dekan:	Prof. Dr. med. dent. Reinhard Hickel
Tag der mündlichen Prüfung:	20.05.2021

1. Affidavit

LMU LUDWIG-MAXIMILIANS-UNIVERSITÄT MÜNCHEN | Promotionsbüro Medizinische Fakultät | MMRS

Eidesstattliche Versicherung

Armbruster, Marco

_____

Name, Vorname

Ich erkläre hiermit an Eides statt, dass ich die vorliegende Dissertation mit dem Titel:

Die Rolle der dynamischen kontrastverstärkten Magnetresonanztomographie in der Evaluation von neuroendokrinen Lebermetastasen

selbständig verfasst, mich außer der angegebenen keiner weiteren Hilfsmittel bedient und alle Erkenntnisse, die aus dem Schrifttum ganz oder annähernd übernommen sind, als solche kenntlich gemacht und nach ihrer Herkunft unter Bezeichnung der Fundstelle einzeln nachgewiesen habe.

Ich erkläre des Weiteren, dass die hier vorgelegte Dissertation nicht in gleicher oder in ähnlicher Form bei einer anderen Stelle zur Erlangung eines akademischen Grades eingereicht wurde.

München, 21.06.2021 Marco Armbruster

_____ _____

Ort, Datum Unterschrift Doktorandin bzw. Doktorand

Inhaltsverzeichnis

AFFIDAVIT..... 3

INHALTSVERZEICHNIS..... 4

ABKÜRZUNGSVERZEICHNIS..... 5

PUBLIKATIONSLISTE..... 6

1. EIGENER BEITRAG ZU DEN PUBLIKATIONEN..... 7

1.1. Beitrag zu Publikation I..... 7

1.2. Beitrag zu Publikation II..... 8

2. ABSTRACT..... 9

3. EINLEITUNG..... 12

3.1. Diagnostische Verfahren bei metastasierten neuroendokrinen Tumoren..... 12

3.2. Aktueller Forschungsstand..... 15

3.3. Fragestellungen der Studie..... 16

3.4. Studiendesign..... 17

3.5. Methodik und statische Auswertung..... 18

4. ZUSAMMENFASSUNG 20

5. PAPER I..... 24

Evaluation of Neuroendocrine Liver Metastases: A Comparison of Dynamic Contrast-Enhanced Magnetic Resonance Imaging and Positron Emission Tomography/Computed Tomography

Investigative Radiology, Volume 49, Number 1, 2014..... p7-14

6. PAPER II..... 25

Diagnostisch Accuracy of Dynamic Gadoxetic-Acid-Enhanced MRI and PET/CT Compared in Patients with Liver Metastases From Neuroendocrine Neoplasms

Journal of Magnetic Resonance Imaging, Volume 40, Issue 2, 2014..... *p457-466*

7. LITERATURVERZEICHNIS..... 26

DANKSAGUNG..... 28

Abkürzungsverzeichnis

APF	Arterial Plasma Flow
AUC	Area Under the Curve
CT	Computertomographie
DCE-MRI	Dynamic Contrast-enhanced Magnetic Resonance Imaging
DICOM	Digital Imaging and Communications in Medicine
FDG	Fluorodesoxyglucose
GEPNET	Gastroenteropankreatische neuroendorkine Tumore
GRE	Gradientenecho
KM	Kontrastmittel
MRT	Mangetresonanztomographie
MTT	Mean Transit Time
NEC	Nneuroendokrine Karzinome
NEN	Neuroendokrine Neoplasien
NET	Neuroendokrine Tumore
PET	Positronen-Emissions-Tomographie
SUV	Specific Uptake Value
VPF	Venous Plasma Flow
TPF	Total Plasma Flow
UF	Uptake Fraction
UR	Uptake Rate

Publikationsliste

Während meiner Tätigkeit als Doktorand am Institut für Klinische Radiologie der Ludwig-Maximilians-Universität München sind unter Betreuung von Prof. Dr. Wieland Sommer und Prof. Dr. med. Christoph Zech nachfolgende wissenschaftliche Veröffentlichungen unter meiner Mitwirkung entstanden. Eine Gesamtliste an Publikationen mit meinem Beitrag ist dem Abschnitt Lebenslauf beigefügt.

Evaluation of Neuroendocrine Liver Metastases: A Comparison of Dynamic Contrast-Enhanced Magnetic Resonance Imaging and Positron Emission Tomography/Computed Tomography

Armbruster M, Sourbron S, Haug A, Zech CJ, Ingrisch M, Auernhammer CJ, Nikolaou K, Paprottka PM, Rist C, Reiser MF, Sommer WH

Investigative Radiology. 2014 Jan;49(1):7-14. doi: 10.1097/RLI.0b013e3182a4eb4a.

Impact Factor 2014: 4.437

Diagnostic Accuracy of Dynamic Gadoxetic-Acid-Enhanced MRI and PET/CT Compared in Patients With Liver Metastases From Neuroendocrine Neoplasms

Armbruster M, Zech CJ, Sourbron S, Ceelen F, Auernhammer CJ, Rist C, Singnurkar A, Reiser MF, Sommer WH

J Magn Reson Imaging. 2014 Aug;40(2):457-66. doi: 10.1002/jmri.24363.

Impact Factor 2014: 3.210

1. Eigener Beitrag zu den Publikationen

1.1. Beitrag zu Publikation I

Für die Publikation „Evaluation of Neuroendocrine Liver Metastases: A Comparison of Dynamic Contrast-Enhanced Magnetic Resonance Imaging and Positron Emission Tomography/Computed Tomography“ bestand mein Beitrag in der Datenauswertung mit Pre- und Postprocessing der DCE-MRT-Datensätze, der Anpassung und Weiterprogrammierung der bestehenden inhouse MR-Perfusionssoftware PMI 0.4, dem Transfer des von Sourbron et al. im Jahr 2012 in Radiology[1] publizierten Dual-Inlet Two-Compartment MR-Perfusionsmodells der Leber mit Anwendung auf unserem Patientenkollektiv, der statistischen Auswertung und Manuskripterstellung.

Hierzu habe ich zunächst die Digital Imaging and Communications in Medicine (DICOM) Daten der eingeschlossenen 42 Patienten aus dem radiologischen Informationssystem (RIS) exportiert, anonymisiert und in der Perfusionssoftware PMI 0.4 importiert. Um das von Sourbron et al. vorgestellte Perfusionsmodell der Leber auf unser Patientenkollektiv anwenden zu können, musste das Modell in der bestehenden Auswertesoftware angepasst und weiterprogrammiert werden, insbesondere um das Delay zwischen Applikation des Kontrastmittels in einer peripheren, cubitalen, peripheren Vene und Anfluten in der A. hepatica propria zu bestimmen und Atemartefakte mittels retrospektivem Gating in dem über 5 Minuten akquirierten Datensatz zu reduzieren. Hierzu habe ich Herrn Prof. Sourbron während eines zweimonatigen Auslandsaufenthaltes in Leeds (UK) im Zeitraum Oktober-Dezember 2012 unterstützt und aktiv an der Programmierung von PMI 0.4 mitgewirkt. Nachfolgend habe ich in allen 42 MRT- und PET-CT Datensätzen Analyseregionen sowohl innerhalb der Lebermetastasen sowie des normalen Leberhintergrundgewebes eingezeichnet

und quantitative MR-Perfusionsparameter (arterial plasma flow, venous plasma flow, total plasma flow, mean-transit-time, extracellular uptake rate und uptake fraction) sowie SUV-Werte bestimmt. Darüber hinaus war ich maßgeblich an der statistischen Auswertung einschließlich der Kalkulationen mittels der Statistik-Software SAS sowie in der Erstellung des Manuskripts beteiligt.

1.2. Beitrag zu Publikation II

Für die Publikation „Diagnostic Accuracy of Dynamic Gadoxetic-Acid-Enhanced MRI and PET/CT Compared in Patients With Liver Metastases From Neuroendocrine Neoplasms“ bestand mein Beitrag ebenfalls in dem Datenmanagement einschließlich RIS-Export, Anonymisierung, Pre- und Postprocessing der DCE-MRT-Datensätze mittels der Perfusions-Software PMI 0.4, der quantitativen Bestimmung der MR-Perfusionsparameter sowie des SUV in Target-Läsionen sowie dem Leberhintergrund, der statistischen Auswertung und der Manuskripterstellung. In Publikation II wurde die diagnostische Genauigkeit der MR-Perfusionsparameter sowie der PET-CT zur Unterscheidung zwischen normalem Lebergewebe und neuroendokrinen Lebermetastasen bestimmt und hierfür auch die Kombination mehrerer Parameter in einer multivariaten, logistischen Regressionsanalyse mit schrittweisem Selektionsalgorithmus getestet und mittels Bootstrapping bei 1000 Iterationen hinsichtlich Overfitting überprüft. Zusammen mit Prof. Wieland Sommer habe ich maßgeblich diese statistischen Auswertungen durchgeführt, wofür ich vorbereitend an der 6-monatigen Weiterbildung “Health in Numbers: Quantitative Methods in Clinical Public Health Research” der Harvard University, edX teilgenommen habe (Final grade: 95%).

2. Abstract

Neuroendocrine neoplasms (NEN) of the gastroenteropancreatic system constitute a heterogeneous group of malignancies of the digestive tract. Given that a large number of these neoplasms do not show clinical symptoms at an early stage of disease and venous drainage of the involved organs is mainly to the portal system, many patients present with hepatic metastases at the time point of initial diagnosis[2,3]. Accurate staging of patients experiencing NEN has substantial prognostic impact with consequences for further management and therapeutic strategies[4]. Existing imaging modalities for hepatic metastases of NENs include contrast-enhanced computed tomography (CT) and magnetic resonance imaging (MRI), scintigraphy and positron emission tomography (PET) as well as sonography, which all have relevant shortcomings regarding clinical issues[3,5] and patient safety[6,7]. One approach that has the potential to overcome these shortcomings is dynamic contrastenhanced MRI (DCE-MRI) of the liver. In this approach a four-dimensional, time-resolved, acquisition of the liver is performed and both time- and location-dependent information about the distribution of liver-specific contrast agent is assessed. With this information it is possible to quantify the microcirculation of the liver[1]. Recent studies report the value of DCE-MRI in focal and diffuse liver lesions and in NEN metastatic to the liver[1,8-10]. However, there are no reports about the correlation of DCE-MRI parameters and the surrogate parameter SUV (specific uptake value) of PET/CT. With respect to the development of hybrid MRI techniques, particularly MRI/PET, the objective of this docotral thesis was to investigate the relationship of functional and metabolic data derived from these two modalities in patients with hepatic NEN metastases and evaluate the diagnostic accuracy of these two imaging modalities - both in comparison and in combination to each other.

The study was designed as a prospective longitudinal study in patients with histologically proven liver metastases from NEN and included 59 examinations from 42 patients in study I and 32 examinations from 32 patients in study II. Following current guidelines[11] all patients underwent both MRI of the liver and whole body PET/CT during routine checkup within a short time-frame between both examinations, in most cases within 24h (81%). Additionally to morphologic standard MRI sequences a perfusion sequence with high temporal resolution was acquired. Perfusion parameters of metastases and background liver tissue were calculated using the dedicated dual-inlet two-compartment perfusion model first published by Sourbron et al.[1] which takes the special physiology of the liver into account. According to this model in each perfusion dataset region of interest were drawn within the hepatic artery and portal vein and hepatic sinusoids as well as hepatocyts were defined as independent compartments. Using fit algorithm the following physiologic perfusion parameters were calculated both in liver metastases and normal appearing liver tissue: arterial, venous and total plasma flow, mean transit time, extracellular volume, intracellular uptake fraction, and temporal uptake rate of contrast media into hepatocyts. Perfusion analysis was done with the inhouse programmed software PMI 0.4.

The first part of this work investigates the correlation of DCE-MRI perfusion parameters and PET/CT SUV – both with ^{18}F-FDG as a biomarker for tumor metabolism and ^{68}Ga-DOTATATE as surrogate parameter for somatostatin receptor status of tumorous tissue. Whereas *arterial plasma flow* and *arterial flow fraction* are negatively correlated to SUV derived from ^{68}Ga-DOTATATE PET/CT, they correlate positively with ^{18}F-FDG PET/CT (Invest Radiol 2014;49: page 13; Figure 3). *Venous plasma flow, total plasma flow, intracellular uptake fraction* and hepatic *uptake rate* of contrast agent show no correlation to PET/CT but discriminate clearly between metastatic and non-metastatic tissue (Invest Radiol 2014;49: page 12; Table 2). Therefore they

add further information to the characterization of liver metastases from NEN in comparison to PET/CT.

The second part of this work investigates the diagnostic accuracy of DCE-MRI and PET/CT for detection of liver metastases of NEN both in comparison and in combination to each other using a multivariate regression model with bootstrap algorithm to account for overfitting. Cut-off-values for the discrimination of metastatic and nonmetastatic liver tissue as well as values for sensitivity, specificity and the area under the curve are provided for perfusion parameters and SUVs (JMRI 2014;40: page 462; Table 2). For DCE-MRI particularly arterial plasma flow and the uptake of contrast agent into hepatocytes seems to be a promising diagnostic marker (JMRI 2014;40: page 463; Figure 3). Combination of several perfusion parameters and the combination of DCE-MRI parameters and SUV increase the diagnostic accuracy (JMRI 2014;40: page 463; Figure 4).

Results of this work imply that both PET/CT and DCE-MRI provide clinically relevant functional information for the evaluation of NEN liver metastases. Particularly in combination DCE-MRI perfusion parameters and SUV derived from PET/CT have the potential to increase diagnostic accuracy and overcome the shortcomings of existing imaging modalities.

3. Einleitung

3.1. Diagnostische Verfahren bei metastasierten neuroendokrinen Tumoren

Neuroendokrine Neoplasien (NEN) des gastroenteropankreatischen Systems sind eine heterogene Gruppe von Tumoren des Verdauungstraktes, welche nach aktueller WHO-Klassifikation in gut-differenzierte, niedrigmaligne neuroendokrine Tumore (NET), sowie gering-differenzierte, hochmaligne neuroendokrine Karzinome (NEC) unterteilt werden[12,13]. Aufgrund ihres häufig indolenten Größenwachstums sind NEN im Frühstadium in den meisten Fällen klinisch inapparent und durch den portalvenösen Abfluss der gastroenteropankreatischen Organe bei Erstdiagnose häufig bereits hepatisch metastasiert[2,3].

Das Vorhandensein von Lebermetastasen besitzt große Relevanz für die Prognose der betroffenen Patienten, da die Lebenserwartung bei NEN in erster Linie durch das Tumorstadium sowie die An- oder Abwesenheit von Fernmetastasen bestimmt wird, wie in einer großen Datenbank mit 35.618 NEN-Fällen gezeigt wurde: So sinkt das 5-Jahres-Überleben bei Vorliegen von Fernmetastasen bei Patienten mit gut- und moderat-differenzierten NEN von ungefähr 82% auf 35%, sowie für Patienten mit gering-differenzierten NEN von ungefähr 38% auf 4%[4]. Ein korrektes Staging der betroffenen Patienten hat somit hohen prognostischen Einfluss und unmittelbare Konsequenzen auf das Patientenmanagement sowie die anfallenden Therapieentscheidungen.

Das Staging umfasst insbesondere bildgebende Verfahren zur Lokalisation des Primarius sowie zur Detektion und Evaluation von Fernmetastasen. Hierbei kommen aktuell die kontrastverstärkte Computertomographie (CT) und Mangetresonanztomographie (MRT), die Ganzkörper-Szintigraphie und Positronen-Emissions-Tomographie (PET)[11,14,15] sowie die Sonografie zur Anwendung. Während Sonografie, CT und MRT vorwiegend morphologische

Charakteristika des Tumors und seiner Absiedlungen analysieren, ist die Szintigraphie und PET in der Lage, in Abhängigkeit des verwendeten Radiotracers, unterschiedliche metabolische und funktionelle Informationen zu erfassen. Nachfolgend werden die in der aktuellen Studie analysierten bildgebenden Verfahren PET-CT, MRT und DCE-MRT vorgestellt.

PET-CT

In der PET-CT werden für das Staging von NEN insbesondere 18F-Fluorodesoxyglucose (FDG) sowie 68Ga-DOTATAE als Radiotracer eingesetzt: Während mit Hilfe des Somatostatin-Analogon 68Ga-DOTATATE das spezifische Expressions-Muster von Somatostatin-Rezeptoren in gut-differenzierte NEN visualisiert und quantifiziert werden kann, kommt 18F-FDG primär in gering-differenzierten Neoplasien zur Anwendung und quantifiziert den Glukoseumsatz und damit die metabolische Tumoraktivität[16]. Die PET-CT liefert somit tumorspezifische und metabolische Informationen[16-18], besitzt im Vergleich zur MRT jedoch eine ungleich höhere Strahlenbelastung, was insbesondere bei jungen Patienten mit multiplen Follow-up Untersuchungen ein kritisches Abwägen zwischen diagnostischem Informationsgewinn und möglichen Spätfolgen erfordert[6,7,19].

MRT

Die MRT wird neben der PET-CT als weiteres bildgebende Verfahren in den Consensus-Richtlinien der *European Neuroendocrine Tumor Society* (ENETS) für den diagnostischen Workup von NEN empfohlen und ist der CT aufgrund eines höheren Weichteilkontrastes insbesondere in der Detektion von kleinen Lebermetastasen überlegen[20]. Als Identifikationsmerkmale sind neben den klassischen MR-morphologischen Charakteristika

von Lebermetastasen zusätzliche NEN-spezifische Erscheinungsbilder wie eine deutliche Hyperintensität der Läsion in T2-gewichteten Bildern sowie eine Hypervaskularität in der arteriellen Phase nach Kontrastmittelgabe beschrieben[21,22]. Die Einführung von Gadolinium-haltigem, leberspezifischem Kontrastmittel, welches in den Hepatozyten akkumuliert und somit den Kontrast zwischen Tumorgewebe und Leberhintergrund erhöht, konnte die diagnostische Genauigkeit der MRT weiter steigern[23-25]. Allerdings existieren für die konventionelle, kontrast-verstärkte MRT bisher nur begrenzte Möglichkeiten zur Beurteilung des Lebergewebes über die reine Morphologie hinaus, was insbesondere für die Evaluation des Therapieansprechens sowie für die Therapieplanung eine entscheidende Limitation darstellt[3,5].

DCE-MRT

Um diese Limitation zu überbrücken wurde in den letzten zwei Dekaden an neuen Akquisitionstechniken wie beispielsweise der MR-Perfusions- und Diffusionsbildgebung geforscht und diese zunehmend in der klinischen Routine etabliert. Eine Technik welche in diesem Zusammenhang zunehmend in das wissenschaftliche und klinische Interesse rückt, ist die dynamische kontrastverstärkte Leber-MRT (DCE-MRI, dynamic contrast-enhanced magnetic resonance imaging). Dieser Technik liegt eine 4-dimensionale, zeitlich aufgelöste, MR-Akquisition der Leber zugrunde, wodurch die zeitliche und räumliche Verteilung von Kontrastmittel erfasst und somit die Mikrozirkulation des Gewebes quantifiziert und verschiedenartige Perfusionsparameter errechnet werden können[1,8,10]. Für die Quantifizierung werden hierfür pharmakokinetischmathematische Modelle herangezogen, welche auf der Anatomie und Physiologie der Leber basieren. Ein Modell, welches unter

Verwendung des leberspezifischen Kontrastmittels Gd-EOB-DTPA (Primovist, Bayer) erstmalig von Sourbron et al. zur Evaluation der Leberfunktion erfolgreich eingesetzt worden ist, ist das 2-Kompartment Uptake-Modell mit den zwei Subsystemen Extra- und Intrazellulärraum sowie einer dualen Blutversorgung über A. hepatica und V. portae[1]. Mithilfe dieses Modells können aus den akquirierten MR-Signalkurven unter Verwendung von mathematischen Algorithmen Perfusionsparameter wie der arterielle und venöse Blutfluss, die Aufnahmerate von Kontrastmittel in die Hepatozyten sowie das extrazelluläre Volumen des Leberparenchyms quantifiziert werden[1]. Die MRT-Leber-Perfusionsbildgebung hat somit das Potential die Limitationen der Morphologie-basierten konventionellen MRT zu überwinden und lokale und globale funktionelle Informationen der Leber zu erfassen.

3.2. Aktueller Forschungsstand

Mehrere aktuelle Studien berichten über das Potential dieses Verfahrens in fokalen und diffusen Leberläsionen sowie in hepatisch metastasierten NEN[8,9]: So berichten Miyazaki et al. in einer Studie mit 20 Patienten mit NEN und hepatischer Metastasierung von einem möglichen Zusammenhang zwischen arterieller Flussfraktion und Therapieansprechen auf eine Octreotid-Therapie (Radiology, 2012), während Koh et al. den quantifizierten arteriellen Blutfluss als möglichen Biomarker zur Früherkennung von Lebermetastasen und primären Lebertumoren identifiziert haben (Magnetic Resonance in Medicine, 2011). Vor diesem Hintergrund stellt sich die Frage, ob sich das Perfusionsverhalten von Metastasen neuroendokriner Tumore mithilfe der DCE-MRI weiter quantifizieren und charakterisieren lässt und welche diagnostische Genauigkeit die DCE-MRI in der Detektion von Leberfiliae bei Patienten mit NEN besitzt. Mit Hinblick auf aktuelle Entwicklungen von hybriden MRT-

Techniken, namentlich dem MR/PET, erscheint es darüber hinaus sinnvoll die erhobenen Perfusionsparametern mit klinisch bereits etablierten Biomarkern wie dem SUV (specific uptake value) der PET-CT zu vergleichen. Folglich definiert sich das Ziel dieser Dissertation darin das Perfusionsverhalten metastatischen Lebergewebes in Patienten mit NEN mithilfe der dynamischen kontrast-verstärkten MRT zu charakterisieren, die erhobenen Perfusionsparameter mit den Funktionsparametern der PET-CT zu korrelieren und übereinstimmende sowie sich ergänzende funktionale Informationen der beiden Modalitäten zu identifizieren. Darüber hinaus soll die diagnostische Genauigkeit beider Verfahren im direkten Vergleich sowie in ihrer Kombination untersucht werden.

3.3. Fragestellungen der vorgestellten Studien

Folgende Aufgaben- / Fragestellungen wurden zur Bearbeitung des Themas formuliert:

1. Identifikation und Evaluation von Perfusions-Biomarkern der dynamischen kontrastverstärkten MRT für die Charakterisierung von metastatischem Gewebe neuroendokrinen Ursprungs.
2. Vergleich der erhobenen Perfusionsparametern mit dem klinisch etablierten Biomarker SUV der PET-CT unter Verwendung des Radiotracer ^{18}F-FDG für schlecht-differenzierte sowie ^{68}Ga-DOTATATE für gut-differenzierte NEN.
3. Vergleich der diagnostischen Genauigkeit von DCE-MRI und PET-CT in der Detektion von Lebermetastasen neuroendokrinen Ursprungs sowie Klärung der Frage, ob eine Kombination beider Verfahren die Sensitivität und Spezifität erhöhen kann.

3.4. Studiendesign

Beide Studien wurden als prospektive longitudinale Kohortenstudie konzipiert. Im Zeitraum Dezember 2008 bis April 2012 wurden insgesamt 59 Untersuchungen von 42 Patienten mit bekannter hepatischer Metastasierung einer histologisch gesicherten NEN in Studie I, sowie 32 Untersuchungen von 32 Patienten in Studie II eingeschlossen. Einschlusskriterien für beide Studien war hierbei eine histologisch gesicherte NEN des gastroenteropankreatischen Systems, vorbekannte hepatische Lebermetastasen neuroendokrinen Ursprungs, ein Nachsorgetermin mit klinischer Indikation sowohl zur Leber-MRT als auch Ganzkörper-PET-CT sowie ein Alter über 18 Jahren. Ausschlusskriterien für beide Studien war das Vorliegen einer Schwangerschaft, das Vorliegen von Kontraindikationen gegen die MRT oder gegen MRT- oder CT-Kontrastmittel oder PET-Tracer, eine Datumsdifferenz größer 14 Tage zwischen dem Untersuchungszeitpunkt der DCE-MRT und PET-CT, eine Läsionsgröße kleiner 20 mm, eine nicht eindeutige Abgrenzbarkeit der A. hepatica propria oder V. portae in den MR-Perfusionsdatensätzen - beispielsweise aufgrund eines thrombotischen Verschlusses, starke Atemartefakte oder eine verspätete Akquisition der Perfusionsmessung mit unvollständigem Datensatz.

Alle Patienten wurden am Interdisziplinären Zentrum für Neuroendokrine Tumoren des Gastro-Entero-Pankreatischen Systems am Klinikum der Universität München (GEPNET-KUM) behandelt und erhielten im Rahmen ihres Nachsorgeprogramms routinemäßig alle 3 Monate eine MRT-Untersuchung zur Bestimmung der Tumorlast sowie ein Ganzkörper-PET-CT zur Suche nach neu aufgetretenen Metastasen in anderen Organsystemen. Das MR-Protokoll wurde im Rahmen dieser Studie um dynamische Serien ergänzt. Das Ethikkomitee des Instituts bewilligte die Studien und die Zustimmung aller Patienten wurde vor der jeweiligen Untersuchung eingeholt.

3.5. Methodik und statistische Auswertung

Für alle eingeschlossenen Patienten wurde während des Studienzeitraums an mindestens einem der Nachsorgetermine sowohl eine PET-CT Untersuchung als auch eine MRT-Untersuchung mit dynamischen Serien (DCE-MRI) erhoben, wobei beide Untersuchungen in den meisten Fällen innerhalb von 24h akquiriert (81%). Für die Ganzkörper-PET-CT Untersuchungen wurde in Abhängigkeit des Tumorgrading sowie des in Voruntersuchungen verwendeten Radiotracer entweder ^{68}Ga-DOTATATE oder ^{18}F-FDG eingesetzt. Alle MRT-Scans wurden bei einer Feldstärke von 3 Tesla durchgeführt. Als Kontrastmittel (KM) wurde das leberspezifische Kontrastmittel Gd-EOB-DTPA eingesetzt. Das MRT Protokoll enthielt neben T1-gewichteten Sequenzen vor Kontrastgabe auch T2-gewichtete Sequenzen sowie dreidimensionale Gradientenechosequenzen (GRE) mit Fettunterdrückung welche 20 Minuten nach KM-Gabe akquiriert wurden. Im Anschluss wurden DCE-MRI Datensätze über einen Zeitraum von 5 Minuten mit einer zeitlichen Auflösung von 2,2 Sekunden akquiriert, d.h. dass alle 2,2 Sekunden ein vollständiger MR-Datensatz der Leber erzeugt wurde. Mithilfe der Inhouse-Software PMI 0.4 (Platform for Research in Medical Imaging) wurden quantitative Maps zur Visualisierung des intrahepatischen Plasmaflusses sowie des Verteilungsvolumen und der mittleren Passagezeit des Kontrastmittels errechnet.

Sowohl in den morphologischen MRT-Sequenzen als auch in den quantitativen PET-CT- und DCE-MRI-Maps wurden jeweils drei zirkuläre Regionen in das Leberhintergrundgewebe sowie in bis zu 3 Metastasen eingezeichnet. In den PET-CT Datensätzen wurde der SUV der jeweiligen Regionen bestimmt. Für die DCE-MRI Datensätze wurde mithilfe eines dedizierten mathematischen Perfusionsmodelles der *arterielle Plasmafluss* (APF), der *venöse Plasmafluss* (VPF), der *Gesamtplasmafluss* (TPF – total plasma flow), die *mittlere extrazelluläre Passagezeit*

(MTT – mean transit time), das *extrazelluläre Volumen*, die *intrazelluläre Aufnahmefraktion* an Kontrastmittel (UF – uptake fraction) sowie die zeitliche *Aufnahmerate* an Kontrastmittel in das Lebergewebe (UR – uptake rate) errechnet. Die quantifizierten Parameter wurden zwischen Leberhintergrundgewebe sowie metastatischem Gewebe verglichen. Zur Bestimmung der diagnostischen Genauigkeit wurden für SUVs und Perfusionsparameter die Fläche unter der Kurve (AUC – area under the curve), die Sensitivität, Spezifität sowie Cutoff-Werte zur Unterscheidung zwischen metastatischem und nicht-metastatischem Gewebe berechnet.

Die einzelnen Perfusions-Parameter sowie der SUV wurden schrittweise einem multivariaten logistischen Regressionsmodell hinzugefügt und jeweils die AUC errechnet, um die kombinierte diagnostische Genauigkeit zu evaluieren.

Die Studienergebnisse zur Korrelation zwischen DCE-MRI Paramtern und PET/CT wurden in dem radiologischen Journal *Investigative Radiology* (Impact Factor 2014: 4.437) unter dem Titel „Evaluation of Neuroendocrine Liver Metastases: A Comparison of Dynamic Contrast-Enhanced Magnetic Resonance Imaging and Positron Emission Tomography/Computed Tomography“ veröffentlicht.

Die Ergebnisse zum Vergleich der diagnostischen Genauigkeit von DCE-MRI und PET/CT im *Journal of Magnetic Resonance Imaging* (Impact Factor 2014: 3.210) wurden unter dem Titel „Diagnostic Accuracy of Dynamic Gadoxetic-Acid-Enhanced MRI and PET/CT Compared in Patients With Liver Metastases From Neuroendocrine Neoplasms“ publiziert.

4. Zusammenfassung der vorliegenden Arbeiten

Neuroendokrine Neoplasien (NEN) des gastroenteropankreatischen Systems sind eine heterogene Gruppe von Tumoren des Verdauungstraktes, welche aufgrund ihrer initialen Symptomarmut sowie ihres venösen Abflussgebietes über die V. portae bei Erstdiagnose häufig bereits hepatisch metastasiert sind[2,3]. Ein korrektes Staging der betroffenen Patienten besitzt hierbei hohen prognostischen Einfluss sowie unmittelbare Konsequenzen auf anfallenden Therapieentscheidungen[4], wobei die etablierten diagnostischen Verfahren, namentlich die kontrastverstärkte CT und MRT, die Szintigraphie und PET/CT sowie die Sonographie hierbei relevante Limitationen in Bezug auf die gestellten klinischen Fragestellungen[3,5] und die Patientensicherheit aufweisen[6,7]. Eine Technik, die in diesem Zusammenhang den morphologischen Informationsgehalt der MRT erweitern könnte und dahingehend in der hier vorgestellten Disseration untersucht wurde, ist die dynamische kontrastverstärkte Leber-MRT (DCE-MRI, dynamic contrast-enhanced magnetic resonance imaging). Dieser Technik liegt eine 4-dimensionale, zeitlich aufgelöste, MR-Akquisition der Leber zugrunde, wodurch die zeitliche und räumliche Verteilung von leberspezifischem Kontrastmittel erfasst und die Mikrozirkulation des Gewebes quantifiziert werden kann[1]. Mehrere aktuelle Studien berichten von dem Potential dieses Verfahrens in fokalen und diffusen Leberläsionen sowie auch in hepatisch metastasierten NEN[1,8-10], jedoch finden sich in der Literatur bisher keine Berichte über die Korrelation von DCE-MRI Perfusionsparametern mit dem Surrogatparameter SUV (specific uptake value) der PET-CT. Mit Hinblick auf die aktuellen Entwicklungen von hybriden MRT-Techniken, namentlich dem MR/PET, war das Ziel der vorgestellten Dissertation daher die Korrelation zwischen den Perfusionsparametern der DCE-MRI sowie den SUVs der PET-CT bei Patienten mit neuroendokrinen Lebermetastasen

sowie die Bestimmung ihrer jeweiligen diagnostischen Genauigkeit sowohl im direkten Vergleich als auch in ihrer Kombination.

Hierzu wurde eine prospektive longitudinale Kohortenstudie im Rahmen des routinemäßigen Follow-ups von Patienten mit histologisch gesicherten, hepatisch metastasierten NEN konzipiert, in die im Zeitraum Dezember 2008 bis April 2012 insgesamt 59 Untersuchungen von 42 Patienten in Studie I sowie 32 Untersuchungen von 32 Patienten in Studie II eingeschlossen wurden[26,27]. Alle eingeschlossenen Patienten erhielten im Rahmen ihrer Nachsorgeuntersuchung entsprechend der Leitlinienempfehlungen[11] in kurzer zeitlicher Aufeinanderfolge und zumeist innerhalb von 24h (81%) sowohl eine Leber-MRT als auch eine PET-CT Untersuchung[26,27]. Zusätzlich zu den morphologischen Standardsequenzen wurden während der Leber-MRT eine zeitlich hochaufgelöste Perfusionssequenzen akquiriert. Entsprechend des von Sourbron et al.[1] beschriebene Dual-Inlet Two-Compartment Perfusionsmodell wurde in den MR-Perfusionsdatensätze und entsprechend der Leberphysiologie die A. hepatica propria sowie V. portae als Blutzufluss definiert und entsprechende Regionen in der Auswertesoftware PMI 0.4 eingezeichnet. Der Lebersinus und des Intrazellulärraums der Hepatozyten wurden als eigenständige Kompartimente definiert und mithilfe von Fit-Algorithmen in den so modellierten Datensätze unterschiedliche physiologische Perfusionsparameter (*arterieller, venöser und totaler Plasmafluss*, *mittlere extrazelluläre Passagezeit*, *extrazelluläres Volumen*, *intrazelluläre Aufnahmefraktion* sowie die zeitliche *Aufnahmerate* an Kontrastmittel) sowohl für metastatisches und nicht-metastatisches Lebergewebe bestimmt.

Der erste Teil dieser Arbeit beschäftigt sich in Publikation I mit der Korrelation der DCE-MRI Perfusionsparametern mit den SUV der PET/CT unter Verwendung von ^{18}F-FDG als Surrogatparameter für den Tumormetabolismus sowie ^{68}Ga-DOTATATE als Surrogatparameter für den Somatostatinrezepetorstatus des Tumorgewebes. Während der *arterielle Plasmafluss* und die *arterielle Flussfraktion* negativ mit SUVs des ^{68}Ga-DOTATATE-PET-CTs korreliert sind, zeigt sich eine positive Korrelation dieser Parameter zum ^{18}F-FDG-PET-CT[26]. Die Perfusionsparameter *venöser Plasmafluss, Gesamtplasmafluss, intrazelluläre Aufnahmefraktion* sowie die zeitliche *Aufnahmerate* an Kontrastmittel in die Leber besitzen keine Korrelation zum PET-CT, obgleich sie sich deutlich zwischen Tumorgewebe und Leberhintergrund unterscheiden[26]. Folglich liegt nahe, dass sie einen zur PET-CT komplementären Informationsgehalt in der Charakterisierung von Lebermetastasen neuroendokrinen Ursprungs besitzen.

Im zweiten Teil der Arbeit wird die diagnostische Genauigkeit der DCE-MRI und PET-CT in der Detektion von Lebermetastasen bei NEN sowohl im direkten Vergleich als auch mithilfe multivariater Regressionsmodelle untersucht. Dies erfolgt mittels einer multivariaten, logistischen Regressionsanalyse und wird anschließend mit einem schrittweisem Selektionsalgorithmus und Bootstrapping hinsichtlich Overfitting überprüft. Für die oben genannten Perfusionsparameter und SUVs werden Cutoff-Werte zur Unterscheidung zwischen metastatischem und nichtmetastatischem Gewebe definiert sowie ihre jeweilige Sensitivität, Spezifität sowie die Fläche unter der Kurve errechnet[27]. Für die DCE-MRI Parameter stellt sich insbesondere der *arterielle Plasmafluss* als auch die *Aufnahmerate* an Kontrastmittel in die Hepatozyten als vielversprechender diagnostischer Marker heraus[27]. Die Kombination mehrerer Perfusionsparameter sowie die Kombination von DCE-MRI-

Parametern und SUVs erhöht darüber hinaus die diagnostische Genauigkeit im Vergleich zu einer Modalität allein[27].

Die Ergebnisse der vorgestellten Arbeit implizieren, dass sowohl die PET-CT als auch die DCE-MRI klinisch relevante funktionale Informationen zur Evaluation von Lebermetastasen neuroendokrinen Ursprungs besitzen und insbesondere in ihrer Kombination das Potential besitzen, die diagnostische Genauigkeit zu erhöhen und die bestehenden Limitationen der etablierten diagnostischen Verfahren zu überwinden.

5. Publikation I:

Evaluation of Neuroendocrine Liver Metastases: A Comparison of Dynamic Contrast-Enhanced Magnetic Resonance Imaging and Positron Emission Tomography/Computed Tomography

Evaluation of Neuroendocrine Liver Metastases

A Comparison of Dynamic Contrast-Enhanced Magnetic Resonance Imaging and Positron Emission Tomography/Computed Tomography

Marco Armbruster, Steven Sourbron, PhD,† Alexander Haug, MD,‡ Christoph J. Zech, MD,§ Michael Ingrisch, MSc,* Christoph J. Auernhammer, MD,¶ Konstantin Nikolaou, MD,* Philipp M. Paprottka, MD,* Carsten Rist, MD,* Maximilian F. Reiser, MD,* and Wieland H. Sommer, MD**

Objectives: The objective of this study was to evaluate the correlation between dynamic gadoxetic acid–enhanced magnetic resonance imaging parameters and specific uptake values (SUVs) derived from ^{18}fluorodeoxyglucose (^{18}F-FDG) and ^{68}Ga-DOTA-Tyr(3)-octreotate (^{68}Ga-DOTATATE) positron emission tomography/computed tomography (PET/CT) in patients with liver metastases of neuroendocrine neoplasms.

Methods: A total of 42 patients with hepatic metastases of neuroendocrine neoplasms were prospectively enrolled and underwent both dynamic contrast-enhanced magnetic resonance imaging (DCE-MRI) and PET/CT, using either ^{18}F-FDG or ^{68}Ga-DOTATATE as tracer. The DCE-MRI was performed at 3 T with gadolinium ethoxybenzyl diethylenetriamine pentaacetic acid acquiring 48 slices every 2.2 seconds for 5 minutes. Three regions of interest (ROIs) representing the liver background and up to 3 ROIs representing metastatic liver tissue were coregistered in the PET/CT and in the DCE-MRI data sets. For each patient, a dedicated dual-inlet, 2-compartment uptake model was fitted to the enhancement curves of DCE-MRI ROIs and perfusion parameters were calculated. Lesion-to-background ratios of SUVs were correlated with corresponding lesion-to-background ratios of the perfusion parameters arterial plasma flow, venous plasma flow, total plasma flow, extracellular mean transit time, extracellular volume, arterial flow fraction, intracellular uptake rate, and hepatic uptake fraction using the Spearman coefficient.

Results: Whereas the lesion-to-background ratios of arterial plasma flow and arterial flow fraction of liver metastases correlated negatively with the lesion-to-background ratios of SUV_{mean} derived from ^{68}Ga-DOTATATE PET/CT ($r = -0.54$, $P < 0.001$; $r = -0.39$, $P < 0.001$, respectively), they correlated positively with the lesion-to-background ratios of SUV_{mean} derived from ^{18}F-FDG-PET/CT ($r = 0.51$, $P < 0.05$; $r = 0.68$, $P < 0.01$, respectively). The lesion-to-background ratios of the DCE-MRI parameters extracellular mean transit time and extracellular volume correlated very weakly with the lesion-to-background ratios of SUV_{mean} from ^{68}Ga-DOTATATE PET/CT, whereas venous plasma flow, total plasma flow, hepatic uptake fraction, and intracellular uptake rate showed no correlation between DCE-MRI and PET/CT.

Conclusions: Both ^{68}Ga-DOTATATE and ^{18}fluorodeoxyglucose PET/CT partially correlate with MRI perfusion parameters from the dual-inlet, 2-compartment uptake model. The results indicate that the paired imaging methods deliver complementary functional information.

Key Words: PET/CT, DCE-MRI, neuroendocrine tumor, liver metastases

(*Invest Radiol* 2014;49: 7–14)

According to the current World Health Organization classification 2010, neuroendocrine neoplasms (NENs) of the gastroenteropancreatic system are classified into well-differentiated neuroendocrine tumors and poorly differentiated, high-grade malignant neuroendocrine carcinomas.[1] Neuroendocrine neoplasms of the gastroenteropancreatic system often present with liver metastases already at the time point of initial diagnosis.[2] The stage of metastatic disease is associated with a high morbidity and mortality. In a major database with 35,618 cases of NEN, the 5-year survival of patients with well- to moderately differentiated neoplasms decreased from approximately 82% to 35% with the presence of distant metastases and from 38% to 4% for poorly differentiated neoplasms.[3] Therefore, accurate staging of patients experiencing NEN has substantial prognostic impact with consequences for further management and therapeutic strategies.

Imaging modalities for hepatic metastases of NENs include contrast-enhanced computed tomography (CT), magnetic resonance imaging (MRI), and positron emission tomography (PET) with various radiotracers. For NEN liver metastases, characteristic magnetic resonance imaging features have been described[4] including markedly hyperintense signal intensity on T2-weighted images and hypervascularity in the arterial phase after contrast agent administration.[5,6] Whereas existing diagnostic imaging methods of contrast-enhanced MRI or CT provide limited evaluation of tissue characteristics beyond morphology, PET examinations provide additional physiological information, depending on the radiotracer. Whereas ^{18}fluorodeoxyglucose (^{18}F-FDG) is primarily used to visualize metabolic activity in poorly differentiated NENs with high proliferation indices, ^{68}Ga-DOTA-Tyr(3)-octreotate (^{68}Ga-DOTATATE) is a somatostatin analog that binds to somatostatin receptors and is especially suited for well-differentiated tumors.[7] A recent study suggests that the use of ^{68}Ga-DOTATATE PET/CT may increase detection sensitivity compared with contrast-enhanced MRI or CT.[8]

Dynamic contrast-enhanced MRI (DCE-MRI) of the liver is capable of detecting perfusion parameters and quantifying the microcirculatory states of the liver parenchyma and of liver lesions.[9–11] Thus, perfusion imaging of the liver can potentially improve the shortcomings of contrast-enhanced MRI and go beyond purely morphologic imaging by providing regional and global information about blood flow and function within the liver.[12] Some articles report the value of gadoxetic acid–enhanced DCE-MRI in focal and diffuse

Received for publication April 22, 2013; and accepted for publication, after revision, July 5, 2013.

From the *Department of Clinical Radiology, University Hospitals-Grosshadern, Ludwig Maximilians University, Munich, Germany; †Division of Medical Physics, University of Leeds, Leeds, United Kingdom; ‡Department of Nuclear Medicine, University Hospitals-Grosshadern, Ludwig Maximilians University, Munich, Germany; §Department of Clinical Radiology, University of Basel, Basel, Switzerland; and ¶Department of Internal Medicine II, Campus Grosshadern, Interdisciplinary Center of Neuroendocrine Tumors of the GastroEnteroPancreatic System, University Hospitals-Grosshadern, Ludwig Maximilians University, Munich, Germany.

Conflict of Interest and Sources of Funding: S.S. is a paid consultant for Bayer-Schering and receives payment for lectures.
C.J.Z. is a paid consultant for Bayer Healthcare and receives payment for lectures.
C.J.A. is a paid consultant for Ipsen, Novartis, Pfizer, Roche, as well as Falk Foundation and receives payment for lectures.
W.H.S. is a paid consultant for Bayer Healthcare and receives payment for lectures.
For the other authors (M.A., M.I., K.N., P.M.P., C.R., M.F.R.): none declared.

Reprints: Wieland H. Sommer, MD, Department of Clinical Radiology, University of Munich, Grosshadern Campus, Marchioninistr 15, 81377 Munich, Germany. E-mail: Wieland.Sommer@med.uni-muenchen.de.

ISSN: 0020-9996/14/4901–0007

liver lesions and in hepatic metastases of NENs.[13–17] However, we have found no reports that correlate specific uptake values (SUVs) of PET/CT and DCE-MRI parameters.

Given the recent development of hybrid MRI techniques, particularly MRI/PET, we see a need to investigate the relationship of functional and metabolic data derived from these 2 different modalities. Early studies examining the potential of MRI/PET report the potential to acquire morphologic, functional, and metabolic information in 1 examination.[18] Young patients with metastatic disease who receive sequential follow-up examinations might especially benefit from this new hybrid technique because the total radiation dose is significantly decreased in MRI/PET compared with PET/CT.[19] A recent study investigated SUV derived from MRI/PET and PET/CT in patients experiencing NEN and reported strong correlations.[20] Whereas the MRI component provided mainly morphologic information, the combination of MRI/PET with perfusion imaging showed potential to add new functional information.[21] Therefore, the aim of the current study was to analyze the association between gadoxetic acid–enhanced DCE-MRI parameters using a dual-inlet, 2-compartment uptake model and SUVs derived from PET/CT, using ^{18}F-FDG and ^{68}Ga-DOTATATE in patients with known liver metastases from NEN.

METHODS

Patient Cohort

Between May 2009 and December 2011, we prospectively examined 42 patients with known hepatic metastases of NEN of various primary tumor sites, both in DCE-MRI and in PET/CT. The local institutional review board approved the study, and informed consent to the study and the DCE-MRI was obtained from all patients before the examinations. The diagnosis of NEN was confirmed histopathologically in all patients. If the origin of the primary tumor site was known, histological diagnosis was provided through resection or biopsy of the primary tumor. For the patients with disease of unknown origin, tissue was obtained through biopsy of liver metastases. Furthermore, in those patients who received the resection or biopsy in our tertiary center, we also obtained Ki-67 labeling index to assess tumor grading.

Data Acquisition

All MRI examinations (59/42 patients) were scheduled as regular follow-up imaging surveillance that are routinely performed every 3 months in our tertiary center for NENs to assess the exact tumor burden of the liver. Furthermore, for assessment of other distant metastases, all patients underwent whole-body PET/CT imaging as part of their routine follow-up imaging, using either ^{18}F-FDG or ^{68}Ga-DOTATATE. Somatostatin analog therapy was not stopped for PET/CT examinations. There was no interval regarding previous treatments. In most cases, DCE-MRI and PET/CT data sets were acquired within 24 hours (81%). All examinations were separated by less than 14 days. Age and sex were recorded for all patients. Furthermore, the primary tumor site of the NEN, the time since the first diagnosis of NEN, and the number of previous therapies were obtained from the patients' records. The patients' hematocrit levels were recorded on the day of the DCE-MRI examination. Overall, 12 patients had more than 1 follow-up examination; those examinations were included in the analysis, and statistical correction for repeated measurements was performed as described in the succeeding paragraphs.

Magnetic Resonance Imaging

Magnetic resonance imaging was performed with a 3.0-T magnet (MAGNETOM Verio; Siemens Healthcare, Erlangen, Germany) by using a 32-channel phased-array body and spine coil. We used an MRI protocol consisting of precontrast sequences including in- and opposed-phased T1-weighted (T1w) images, postcontrast sequences including T2-weighted imaging, as well as coronal and transverse T1w 3-dimensional (3D) gradient-recalled echo (GRE) images with fat saturation 20 minutes after the contrast injection.

In addition, DCE-MRI data were acquired using a 3D T1w spoiled gradient-echo sequence that was accelerated using view sharing and parallel imaging (time-resolved angiography with stochastic trajectories). Imaging parameters were as follows: repetition time (TR)/echo time (TE), 2.37/0.83 milliseconds; flip angle, 15 degrees; matrix, 192 × 192; parallel acquisition technique factor 4 with a generalized autocalibrating partially parallel acquisition algorithm with 24 reference lines; number of slices, 48; slice thickness, 4 mm; phase/slice oversampling, 17%/25%; field of view, 400 mm; phase field of view, 100%; phase/slice resolution, 100%/63%; partial Fourier, 7/8; central region A, 20%; and sampling density B, 25%. Total acquisition time of DCE-MRI was 5 minutes. Temporal resolution was 2.2 seconds.

As contrast agent, 0.1 mL/kg of gadolinium ethoxybenzyl diethylenetriamine pentaacetic acid (Gd-EOB-DTPA) (Primovist; Bayer Healthcare, Germany) was injected via the antecubital vein with a flow of 2 mL/s 10 seconds after starting the acquisition and flushed with 30 mL saline at the same rate. The patients were instructed to breathe shallowly during the acquisition.

Positron Emission Tomography/Computed Tomography

All PET/CT examinations were part of the clinical routine follow-up imaging protocol of patients with NEN. The patients were examined with either ^{68}Ga-DOTATATE or ^{18}F-FDG, depending on the tumor grading and the tracer used in previous PET/CT examinations as described in the following section: If the examination was the first PET/CT examination of a patient, ^{68}Ga-DOTATATE was used in tumors with low (G1; Ki67 ≤2%), intermediate (G2; 2% < Ki67 < 20%), or unknown proliferation indices,[22] whereas ^{18}F-FDG was used in tumors with high proliferation (G3; Ki67 ≥ 20%) indices.[23,24] In case that a patient received previous examinations, the previously used tracer was retained to provide for better follow-up interpretation.

^{68}Ga-DOTATATE was prepared as described earlier.[25,26] Whole-body PET scans were acquired in 3D mode with 3 minutes per bed position using a Biograph 64 TruePoint PET/CT scanner (Siemens Healthcare, Erlangen, Germany). The emission sequence was started approximately 60 minutes after the intravenous injection of 200 MBq of ^{68}Ga-DOTATATE or ^{18}F-FDG, similar to protocols used in other studies working with ^{68}Ga-labeled somatostatin analogs[24,25,27] or ^{18}F-labeled glucose tracers.[28,29] Emission data were reconstructed with attenuation correction on the basis of low-dose CT (20 mA; 140 kV; matrix, 512 × 512). All imaging procedures were performed in combination with a diagnostic CT scan (100–190 mA s, depending on the region of the scanned organ; 120 kV; collimation, 2.5 mm; pitch, 1.5) of the head, the thorax, the abdomen, and the pelvis performed after a 2.5 mL/s intravenous injection of an iodinated contrast agent (Iomeprol 350 mg/mL; Bracco SpA, Milan, Italy; 1.5 mL/kg body weight). The scan was begun 50 seconds after the contrast injection to depict the portal-venous phase of enhancement.

Postprocessing

Dynamic Contrast-Enhanced Magnetic Resonance Imaging

All DCE-MRI data were postprocessed using the software PMI 0.4 (Platform for Research in Medical Imaging), written in-house

in IDL6.4 (ITT, Boulder, CO).[11,30,31] Contrast agent concentrations were approximated by the relative signal enhancement.[32] Arterial and venous blood concentrations were converted to plasma concentrations using the patients' hematocrit.

First semiquantitative maps including maximum signal intensity enhancement, time-to-peak, and area under the curve were calculated by subsuming the information from all acquired data sets for each slice. The arterial input function was defined inside the lumen of the abdominal aorta on a maximum enhancement map. Therefore, a radiologist with 5 years' experience in abdominal imaging and DCE-MRI broadly circumscribed the aorta above the renal arteries by drawing a region of interest (ROI) on 3 or 4 adjacent slices. To select only the voxels clearly within the aorta, this ROI was shrunk automatically by extracting the pixels in the top 10% of the value range. Quantitative maps including plasma flow, volume of distribution, and mean transit time were calculated by deconvolving tissue concentrations with the arterial input function.[31,33,34] The venous input function was then defined on a plasma flow map by drawing a ROI around both intrahepatic and extrahepatic portions of the portal vein on 3 or 4 adjacent slices. This ROI was also shrunk by selecting the pixels in the top 10% of the value range.[11] The complete 4-parameter dual-inlet, 2-compartment uptake model, with arterial delay correction, was fitted to all defined ROIs representing metastatic or background liver tissue (provided in the succeeding paragraphs). This model was used because it takes the special pharmacokinetic properties of the hepatobiliary contrast agent Gd-EOB-DTPA into account and has been recently validated for this purpose by Sourbron et al.[11] The following perfusion parameters were calculated: arterial plasma flow (APF), venous plasma flow (VPF), total plasma flow (TPF), extracellular mean transit time (exMTT), extracellular volume (exVol), arterial flow fraction (AFF), intracellular uptake rate (UR), and hepatic uptake fraction (UF).

Definition of ROIs in PET/CT and DCE-MRI Data Sets

For each patient, 3 regions representing liver background tissue and up to 3 viable metastases with diameters greater than 20 mm were identified on coronal PET/CT data sets and DCE-MRI semiparametric maps. To confirm whether identified lesions correspond to metastases rather than to the liver background, information from delayed coronal T1w GRE sequences 20 minutes after the contrast injection of Gd-EOB-DTPA, diffusion-weighted imaging, contrast-enhanced T1w sequences, and T2-weighted sequences were taken into account. The ROIs representing the liver background were drawn as circles with diameters of 15 to 20 voxels. The ROIs representing the metastases included the entire lesion with the exception of central nonenhancing areas that likely represented central necrosis.

The DCE-MRI and PET/CT data sets were coregistered using anatomic landmarks and distances from the ROI to the landmarks, standardized as follows: the origin of the renal arteries was defined in PET/CT and DCE-MRI mean transit time semiparametric maps. The ROIs were manually first defined in the PET/CT data sets. Corresponding distances in *x*, *y*, and *z* planes from the anatomic landmarks were calculated using Digital Imaging and Communications in Medicine (DICOM)-header information (slice thickness and slice margin). The DCE-MRI ROIs were then defined according to the PET/CT ROIs, the calculated distances from the anatomic landmarks, and the morphologic information from T1 sequences obtained 20 minutes after the contrast medium injection.

Normalization of SUV and DCE-MRI parameters of metastases to liver background

To diminish the influence of examination-based data, we calculated the relative tracer uptake of metastases by dividing the SUV of metastases by the mean SUV of 3 ROIs representing normal-appearing liver tissue (lesion-to-background ratio).[35,36] This was performed accordingly for all DCE-MRI parameters.

Statistical Analysis

Statistical analyses were performed using commercially available software (SAS 9.3; SAS Institute Inc, Cary, NC). To confirm whether continuous variables were normally distributed, the Kolmogorov-Smirnov test was applied for SUV, APF, VPF, TPF, exVol, exMTT, AFF, UF, and UR. Variables following normal distribution are reported as mean (SD). To examine whether normally distributed variables were different between the metastases and the liver background, the Student *t* test for independent samples was applied to test for differences in means. In case of nonnormal distribution, the Wilcoxon rank sum test was used.

Dynamic contrast-enhanced magnetic resonance imaging perfusion parameters of metastases were normalized to liver background and correlated to the corresponding relative SUV_{mean} using the Spearman coefficient with Fisher z-transformation. These analyses were calculated separately for examinations using ^{18}F-FDG or ^{68}Ga-DOTATATE. The SUV_{mean} was used instead of SUV_{max} to facilitate a comparison between the PET/CT and DCE-MRI parameters because the DCE-MRI parameters were based on mean values. A generalized estimating equation (GEE) model cluster analysis was then performed to estimate the statistical effect of multiple measurements within the same data set (multiple lesions per examination and multiple examinations per patient).

RESULTS

Patient Characteristics

The mean (SD) age of the study population was 59.8 (9.9). The primary tumor sites of the NEN were pancreas (n = 10), ileum (n = 9), jejunum (n = 7), colon (n = 6), stomach (n = 4), and lung (n = 1). Tumor origin was unknown in 5 patients. Many patients had received histopathological evaluation in other hospitals. Therefore, the Ki-67 index was not determined in all patients. Most of the patients had multiple previous treatments: transarterial radioembolization using ^{90}yttrium (n = 27), somatostatin analog therapy with ocreotide or lanreotide (n = 17), peptide receptor radionuclide therapy using ^{177}lutetium-DOTA-TATE and ^{90}yttrium-DOTA-TATE (n = 16), chemotherapy (n = 12), hemihepatectomy (n = 8), transarterial chemoembolization (n = 5), or radiofrequency ablation (n = 1) (Table 1).

Of 59 DCE-MRI examinations, 17 were excluded from the analysis because no lesions with diameters greater than 20 mm could be defined on either PET/CT or DCE-MRI images (n = 5), the venous input function could not be clearly identified (n = 3), acquisition was incorrect because of strong motion artifacts (n = 6), or delayed start of DCE-MRI sequence (n = 3). Among the 42 remaining examinations, there were 31 examinations with ^{68}Ga-DOTATATE-PET as tracer and 11 examinations with ^{18}F-FDG-PET as tracer (Fig. 1).

A total of 92 ROIs could be defined in the metastases and a total of 126 ROIs could be defined in the normal-appearing liver tissue on both DCE-MRI and PET/CT images.

Differentiation Between the Metastases and the Liver Background

Figure 2 shows the appearance of the metastases and the liver background in DCE-MRI, PET/CT, and T1w 3D GRE sequences.

The following parameters exhibited significantly different values for the metastatic tissue compared with liver background: SUV_{mean} derived from ^{68}Ga-DOTATATE PET/CT and from ^{18}F-FDG PET/CT, APF, VPF, TPF, exVol, AFF, UF, and UR. Detailed values are provided in the succeeding sections.

TABLE 1. Patient and Clinical Characteristics of the Study Cohort (n = 42)

Characteristic	n
Sex	
Male	21
Female	21
Primary tumor site	
Pancreas	10
Ileum	9
Jejunum	7
Colon	6
Stomach	4
Lung	1
Unknown	5
Histopathologic tumor grading	
G1 (Ki-67 ≤2%)	4
G2 (2% < Ki-67 < 20%)	10
G3 (Ki-67 ≥ 20%)	5
Unknown	23
Previous therapies	
TARE (^{90}yttrium)	27
Somatostatin analog therapy	17
PRRT (^{117}lutetium + ^{90}yttrium)	16
Chemotherapy	12
Hemihepatectomy	8
TACE	5
RFA	1

The mean (SD) age was 59.8 (9.9) y (age range, 42–80 y).

PRRT indicates peptide receptor radionuclide therapy; RFA, radiofrequency ablation; TARE, transarterial radioembolization; TACE, transarterial chemoebolization.

Positron Emission Tomography/Computed Tomography Findings

The SUV_{mean} (SD) from ^{68}Ga-DOTATATE PET/CT was significantly higher for the metastases (17.09 [8.99]; n = 72) than for the liver background (4.78 [1.52]) ($P < 0.001$). The SUV_{mean} (SD) from ^{18}F-FDG PET/CT was also higher for the liver metastases (9.79 [5.31]; n = 20) than for the ROIs representing normal liver tissue (2.25±0.71) ($P < 0.001$).

Dynamic Contrast-Enhanced Magnetic Resonance Imaging Findings

The metastases showed a significantly higher APF (65.11 [55.82] mL/min per 100 mL; n = 92) compared with the normal liver tissue (19.16 [17.59] mL/min per 100 mL) ($P < 0.001$), whereas the VPF rates were significantly lower for the metastases (10.30 [27.77] mL/min per 100 mL; n = 92) than for the liver background (33.80 [31.53] mL/min per 100 mL) ($P < 0.001$). The total plasma flow (APF + VPF) was increased up to 42% in the metastases (75.41 [75.63] mL/min per 100 mL; n = 92) compared with the ROIs representing the liver background (52.96 [35.57] mL/min per 100 mL) ($P < 0.001$).

The AFF was significantly higher in the metastases (90.64% [17.30%]; n = 92) than in the normal liver tissue (42.36% [30.97%]) ($P < 0.001$). Also, the mean exVol was significantly higher for the lesions (21.50 [14.06] mL per 100 mL; n = 92) than for the normal liver tissue (15.06 [8.4]1 mL per 100 mL) ($P < 0.001$), whereas the exMTT did not differ significantly (19.84 [8.53] seconds; n = 92 vs 19.11 [10.35] seconds) ($P = 0.236$).

The UR of Gd-EOB-DTPA was significantly different between the metastases and the liver background ($P < 0.001$) and was significantly lower for the metastases (2.02 [3.27] per 100 mL/min; n = 92) than for the normal liver tissue ROIs (3.37 [2.05] per 100 mL/min).

The UF of Gd-EOB-DTPA, too, was significantly lower for the metastases (2.81% [2.33%]; n = 92) than for the liver background (7.67% [5.53%]) ($P < 0.001$).

Correlation Analysis of Lesion-to-Background Ratios of Metastases in SUV From the PET/CT and DCE-MRI Parameters

^{68}Ga-DOTA-Tyr(3)-octreotate

Table 2 shows the results of correlations between SUV_{mean} derived from ^{68}Ga-DOTATATE PET/CT and DCE-MRI parameters: whereas the lesion-to-background ratios of SUV_{mean} correlated significantly negative to the lesion-to-background ratios of APF values ($r = -0.54$; $P < 0.001$; 95% confidence interval [CI], −0.69 to

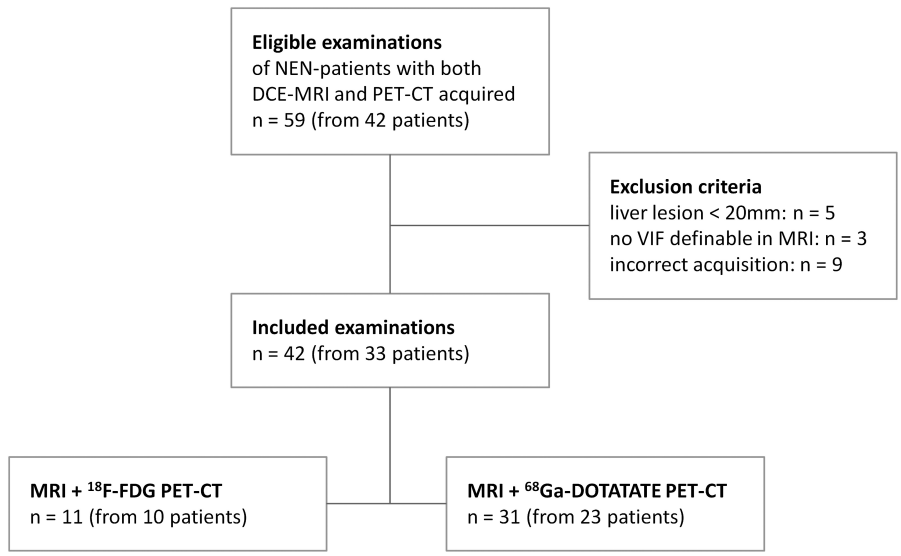

FIGURE 1. Flow chart of study profile. VIF indicates venous input function.

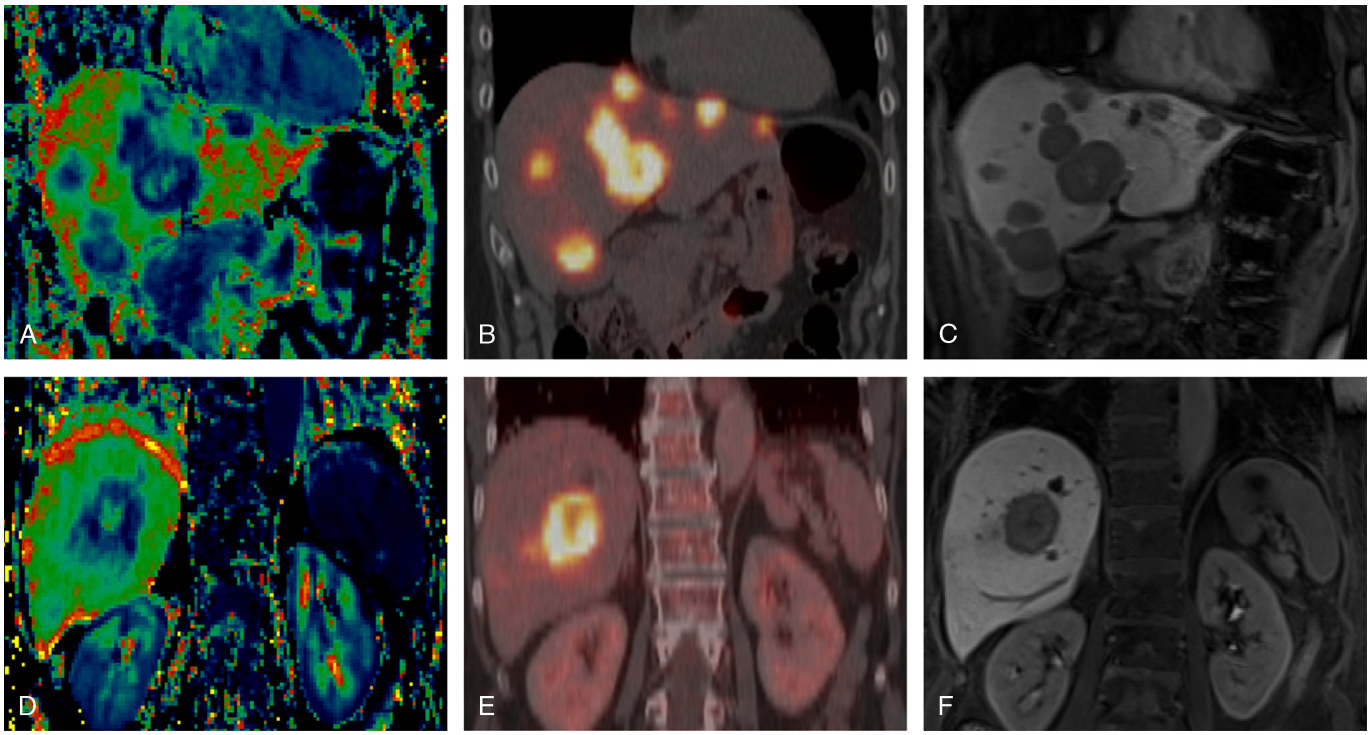

FIGURE 2. Metastatic liver tissue in patients experiencing NENs. A to C, Coronal images through the mean transit time semiparametric map of the DCE-MRI data set (A), the corresponding fused images of the PET/CT (B), and T1w 3D GRE sequence in the hepatobiliary phase (20-minute postcontrast injection; TR, 2.37 milliseconds; TE, 0.83 milliseconds; flip angle, 15 degrees) (C) in a 65-year-old woman with multiple metastases. The tracer used in this PET/CT examination was ^{68}Ga-DOTATATE. D to F, Coronal images through the mean transit time semiparametric map of the DCE-MRI data set (D), the corresponding fused images of the PET/CT (E), and T1w 3D GRE sequence in the hepatobiliary phase (20-minute postcontrast injection; TR, 2.37 milliseconds; TE, 0.83 milliseconds; flip angle, 15 degrees) (F) in a 79-year-old woman with hepatic metastases. The tracer used in this PET/CT examination was ^{18}F-FDG. A visual comparison between the MTT semiparametric map and the PET/CT indicates a good visual correlation between DCE-MRI and PET/CT with both radiotracers to differentiate between the lesions and the liver background. The images in the hepatobiliary phase allow a precise evaluation of morphologic information, for example, lesion size and detection of small satellite metastases.

−0.36) and of AFF ($r = -0.39$; $P < 0.001$; 95% CI, −0.57 to −0.17) (Fig. 3), the lesion-to-background ratios of SUV_{mean} showed a significant positive correlation to relative exMTT ($r = 0.29$; $P = 0.012$; 95% CI, 0.07–0.49) and to exVol ($r = 0.27$; $P = 0.024$; 95% CI, 0.04–0.47). The GEE-model cluster analysis of the lesion-to-background ratios of APF, AFF, exVol, and exMTT versus the lesion-to-background ratios of SUV_{mean} confirmed the significant results after correction for multiple measurements per patient. The lesion- to-background ratios of the remaining DCE-MRI values (VPF, TPF, UF, and UR) did not show significant correlation with SUV_{mean}.

^{18}Fluorodeoxyglucose

The lesion-to-background ratios of SUV_{mean} showed a significantly positive correlation to APF ($r = 0.51$; $P = 0.037$; 95% CI, 0.02–0.80) and AFF ($r = 0.68$; $P = 0.002$; 95% CI, 0.28–0.88) (Fig. 3). Results of a GEE-model cluster analysis corrected for the multiple measurements per patient confirmed the significance of the correlations. The lesion-to-background ratios of the remaining DCE-MRI values (VPF, TPF, exMTT, exVol, UF, and UR) did not show significant correlation with SUV_{mean} (Table 2).

DISCUSSION

In the current study, we analyzed the association between DCE-MRI parameters and SUV from PET/CT using different radiotracers. We showed that the perfusion parameters derived from DCE-MRI and the SUVs derived from PET/CT using ^{68}Ga-DOTATATE and ^{18}F-FDG differ significantly between the liver background and the liver metastases. In a further analysis to determine associations between SUV and DCE-MRI, we found a negative correlation between APF and SUV_{mean} derived from ^{68}Ga-DOTATATE-PET/CT but a positive correlation between APF and SUV_{mean} derived from ^{18}F-FDG-PET/CT. Interestingly, VPF, TPF, UF, and UR did not show correlations with SUV_{mean} derived from ^{68}Ga-DOTATATE or ^{18}F-FDG, although these parameters showed significant differences between metastatic and background liver tissues. These findings might be relevant to the current trend toward hybrid imaging techniques and indicate that the combination of techniques such as MRI/PET may provide additional functional and metabolic information because probably different aspects of liver function are measured using both modalities.

The significant correlations, which we found in our study, can be interpreted using physiologic mechanisms. We showed that both APF ($r = -0.54$) and AFF ($r = -0.39$) correlate significantly negative to SUV_{mean} derived from PET/CT with ^{68}Ga-DOTATATE as tracer and implied that lesions with a relatively high arterial perfusion show a relatively low expression of somatostatin receptors and therefore less specific uptake of ^{68}Ga-DOTATATE. Kayani et al[24] showed, in a series of 38 consecutive patients, that there is a greater uptake of ^{68}Ga-DOTATATE in low-grade NEN compared with high-grade NEN (median SUV, 29 vs 4.3, $P = 0.0033$). Thus, one possible

TABLE 2. The Spearman Correlation Analysis of Lesion-to-Background Ratios Derived From PET/CT and DCE-MRI

		PET/CT Correlation Parameters	
		SUV_{mean} from ^{68}Ga-DOTATATE PET	SUV_{mean} from ^{18}F-FDG PET
DCE-MRI correlation parameters	APF, mL/min per 100 mL	**−0.54* (−0.69 to −0.36)†**	**0.51 (0.02 to 0.8)**
		***P* < 0.001**	***P* < 0.05**
	VPF, mL/min per 100 mL	0.08 (−0.15 to 0.31)	−0.07 (−0.55 to 0.44)
		n.s.	n.s.
	TPF, mL/min per 100 mL	−0.11 (−0.33 to 0.13)	−0.47 (−0.78 to −0.04)
		n.s.	n.s.
	Extracellular MTT, s	**0.29 (0.07 to 0.49)**	0.25 (−0.28 to 0.67)
		***P* < 0.05**	n.s.
	Extracellular volume, mL/100 mL	**0.27 (0.04 to 0.47)**	−0.48 (−0.79 to 0.02)
		***P* < 0.001**	n.s.
	Arterial flow fraction, %	**−0.39 (−0.57 to −0.17)**	**0.68 (0.28 to 0.88)**
		***P* < 0.001**	***P* < 0.01**
	Uptake fraction, %	0.16 (−0.07 to 0.38)	0.42 (−0.10 to 0.76)
		n.s.	n.s.
	Uptake rate, 100 per min	0.09 (−0.14 to 0.32)	0.14 (−0.38 to 0.59)
		n.s.	n.s.

Significant correlations are set in boldface.

* The Spearman coefficient.

† 95% confidence intervals.

^{18}F-FDG indicates ^{18}fluorodeoxyglucose; ^{68}Ga-DOTATATE, ^{68}Ga-DOTA-Tyr(3)-octreotate; APF, arterial plasma flow; CT, computed tomography; DCE-MRI, dynamic contrast-enhanced magnetic resonance imaging; MTT, mean transit time; n.s., not significant; PET, positron emission tomography; SUV, specific uptake value; TPF, total plasma flow; VPF, venous plasma flow.

explanation for the negative correlation between APF and SUV_{mean} in our study might be a correlation between DCE-MRI parameters and tumor grading. To our knowledge, there are no reports in the literature on the role of perfusion of neuroendocrine tumor metastases and tumor grading, but similar correlations have been described for renal cell carcinoma. In a study with 21 patients, Palmowski et al[37] reported significantly higher DCE-MRI perfusion values (P<0.05) in high-grade tumors than in intermediate-grade tumors. Unfortunately, our sample size for Ki-67 was not sufficient to prove this trend. Further research is needed to investigate the interdependency between tumor grading and tumor perfusion in NENs.

We also reported that APF (r = 0.51) and AFF (r = 0.68) are positively correlated to the SUV_{mean} derived from PET/CT with ^{18}F-FDG as tracer and suggest that metabolic activity is linked, either directly or indirectly, to arterial perfusion. Kayani et al[24] were able to show that, conversely to ^{68}Ga-DOTATATE, there is a higher uptake of ^{18}F-FDG in high-grade NEN compared with the uptake in low-grade NEN (median SUV, 11.7 vs 2.9). Thus, the positive correlation between DCE-MRI parameters and SUV from ^{18}F-FDG-PET/CT may also be associated with tumor grading. The association between glucose metabolism and arterial perfusion could also be attributed to biochemical mechanisms. There is evidence that metastatic tissue has impaired oxidative phosphorylation and increased glycolytic rate and lactate production,[38–41] culminating in increased apoptosis and tumor proliferation.[42] Because anaerobic glycolysis extracts less adenosine triphosphates from glucose molecules than aerobic glycolysis does, there is a higher need for blood supply of glucose in metastatic tissue. This can be achieved either through increased perfusion or through increased extraction fraction of glucose. The latter mechanism could be shown in DCE-MRI in patients with arterial wall in flammation,[43] whereas our results suggest that higher metabolic activity is also associated with increased perfusion. Further studies should aim to explore and quantify the effect of those mechanisms in oncologic patients.

The APF and AFF of NEN metastatic to the liver seem to be surrogate markers for metabolic activity and associated with expression of somatostatin receptors. Therefore, APF and AFF seem relevant to the diagnosis and monitoring of liver metastases. Other DCE-MRI parameters (exMTT and exVol) showed weak correlations to somatostatin receptor status. Still, other DCE-MRI parameters (VPF, TPF, UF, and UR) showed different values for the metastases and the normal liver tissue but did not correlate with SUV, using ^{18}F-FDG or ^{68}Ga-DOTATATE, probably related to different physiologic mechanisms measured through PET/CT and DCE-MRI. Therefore, these parameters might have the potential to provide additional information.

Given the current research on therapy-related response assessment in targeted therapies, our results suggest that several DCE-MRI parameters may be potential imaging biomarkers and may provide important information. It should be the aim of future studies to analyze the effect of different treatments on these DCE-MRI parameters and refine which are best suited to monitor treatment response.

We used a dedicated dual-inlet, 2-compartment model with the hepatobiliary contrast agent gadoxetic acid for our DCE-MRI examinations. The technique allowed us to obtain the full range of functional parameters from the time-resolved data acquisition with a detailed morphologic assessment in the hepatobiliary phase in T1w 3D GRE sequences with fat saturation (Fig. 2) in 1 comprehensive magnetic resonance examination and only 1 application of a standard dose of contrast agent. Whereas a conventional 1- or 2-compartment model may show inaccurate results because of the physiological properties of gadoxetic acid, the model used in our study was specially designed and validated for this purpose.[11] The low uptake fraction in metastases in the absence of organic anion transporting polypeptide receptors can be explained through interstitial uptake because of the extracellular properties of gadoxetic acid.

The data from our study must be interpreted in the context of the study design. Our patients with NEN metastatic to the liver had long intervals since primary diagnosis and received a variety of

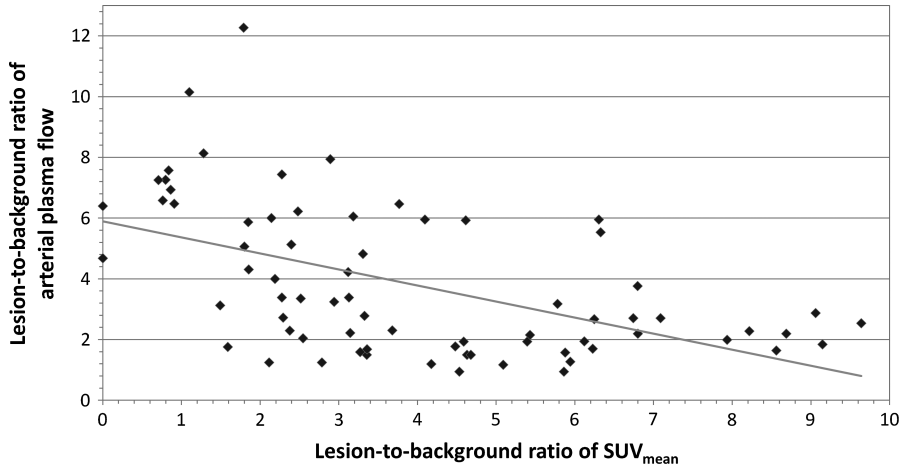

A Correlation Plot ^{68}Ga-DOTATATE PET/CT vs. Arterial Plasma Flow

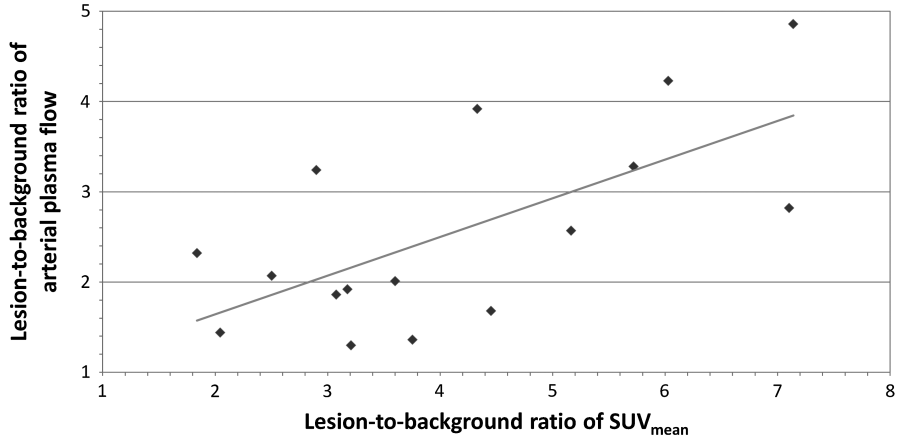

B Correlation Plot ^{18}F-FDG PET/CT vs. Arterial Plasma Flow

FIGURE 3. Correlation plots of PET/CT versus DCE-MRI. A, Scatterplot and linear regression line of the relative SUV_{mean} derived from ^{68}Ga-DOTATATE PET/CT versus the relative APF derived from DCE-MRI for the metastases. There is a significantly negative correlation ($r = -0.54$; $P < 0.001$). B, Scatterplot and linear regression line of relative SUV_{mean} derived from ^{18}F-FDG PET/CT versus the relative APF derived from DCE-MRI for the metastases. There is a significant positive correlation ($r = 0.51$; $P = 0.05$).

previous therapies. Embolizing therapies, especially radioembolization and transarterial chemoembolization, might influence DCE-MRI parameters such as the APF and the AFF of the metastases. For PET/CT examinations, medication with somatostatin analog was not stopped and there was no interval regarding previous octreotid therapies. However, Haug et al[44] showed, in a study of 105 patients, that treatment with somatostatin analog does not affect tumor uptake of ^{68}Ga-DOTATATE in patients with NEN. Future studies might focus on the association between DCE-MRI parameters and SUV from PET/CT in patients with an initial diagnosis of different types of tumors in the absence of previous therapies. For the definition of the ROIs, we did not have histopathologic correlation. Because NEN may have diffuse liver involvement, even normal-appearing liver tissue may be infiltrated by microscopic tumor invasion. However, we tried to avoid any misclassification by correlation with all available morphologic sequences.

CONCLUSIONS

In conclusion, we were able to show that some DCE-MRI parameters, especially the flow-related, are correlated with SUV from PET/CT, whereas other parameters correlate poorly or not at all, suggesting that the combination of MR and PET may improve the diagnostic power compared with each technique individually and has the potential to provide additional functional information of the liver.

ACKNOWLEDGMENTS

The authors thank Allan Paris, DO (Battle Creek, MI), for his contribution and editing of the manuscript.

REFERENCES

1. Anlauf M. Neuroendocrine neoplasms of the gastroenteropancreatic system: pathology and classification. *Horm Metab Res*. 2011;43:825–831.
2. Auernhammer CJ, Goke B. Therapeutic strategies for advanced neuroendocrine carcinomas of jejunum/ileum and pancreatic origin. *Gut*. 2011;60:1009–1021.
3. Yao JC, Hassan M, Phan A, et al. One hundred years after "carcinoid": epidemiology of and prognostic factors for neuroendocrine tumors in 35,825 cases in the United States. *J Clin Oncol*. 2008;26:3063–3072.
4. Rockall AG, Reznek RH. Imaging of neuroendocrine tumours (CT/MR/US). *Best Pract Res Clin Endocrinol Metab*. 2007;21:43–68.
5. Debray MP, Geoffroy O, Laissy JP, et al. Imaging appearances of metastases from neuroendocrine tumours of the pancreas. *Br J Radiol*. 2001;74:1065–1070.

6. Dromain C, de Baere T, Baudin E, et al. MR imaging of hepatic metastases caused by neuroendocrine tumors: comparing four techniques. *AJR Am J Roentgenol*. 2003;180:121–128.
7. Rufini V, Baum RP, Castaldi P, et al. Role of PET/CT in the functional imaging of endocrine pancreatic tumors. *Abdom Imaging*. 2012;37:1004–1020.
8. Frilling A, Sotiropoulos GC, Radtke A, et al. The impact of 68Ga-DOTATOC positron emission tomography/computed tomography on the multimodal management of patients with neuroendocrine tumors. *Ann Surg*. 2010;252:850–856.
9. Materne R, Smith AM, Peeters F, et al. Assessment of hepatic perfusion parameters with dynamic MRI. *Magn Reson Med*. 2002;47:135–142.
10. Koh TS, Thng CH, Lee PS, et al. Hepatic metastases: in vivo assessment of perfusion parameters at dynamic contrast-enhanced MR imaging with dual-input two-compartment tracer kinetics model. *Radiology*. 2008;249:307–320.
11. Sourbron S, Sommer WH, Reiser MF, et al. Combined quantification of liver perfusion and function with dynamic gadoxetic acid-enhanced mr imaging. *Radiology*. 2012;263:874–883.
12. Pandharipande PV, Krinsky GA, Rusinek H, et al. Perfusion imaging of the liver: current challenges and future goals. *Radiology*. 2005;234:661–673.
13. Miyazaki K, Orton MR, Davidson RL, et al. Neuroendocrine tumor liver metastases:use of dynamic contrast-enhanced MR imaging to monitor and predict radiolabeled octreotide therapy response. *Radiology*. 2012;263:139–148.
14. Koh TS, Thng CH, Hartono S, et al. Dynamic contrast-enhanced MRI of neuroendocrine hepatic metastases: a feasibility study using a dual-input two-compartment model. *Magn Reson Med*. 2011;65:250–260.
15. Kim YK, Lee MW, Lee WJ, et al. Diagnostic accuracy and sensitivity of diffusion-weighted and of gadoxetic acid-enhanced 3-T MR imaging alone or in combination in the detection of small liver metastasis (≤ 1.5 cm in diameter). *Invest Radiol*. 2012;47:159–166.
16. Motosugi U, Ichikawa T, Onohara K, et al. Distinguishing hepatic metastasis from hemangioma using gadoxetic acid-enhanced magnetic resonance imaging. *Invest Radiol*. 2011;46:359–365.
17. Seo HJ, Kim MJ, Lee JD, et al. Gadoxetate disodium-enhanced magnetic resonance imaging versus contrast-enhanced 18F-fluorodeoxyglucose positron emission tomography/computed tomography for the detection of colorectal liver metastases. *Invest Radiol*. 2011;46:548–555.
18. Schwenzer NF, Schmidt H, Claussen CD. Whole-body MR/PET: applications in abdominal imaging. *Abdom Imaging*. 2012;37:20–28.
19. Schwenzer NF, Pfannenberg C, Reischl G, et al. Application of MR/PET in oncologic imaging [in German]. *Rofo*. 2012;184:780–787.
20. Gaertner FC, Beer AJ, Souvatzoglou M, et al. Evaluation of feasibility and image quality of 68Ga-DOTATOC positron emission tomography/magnetic resonance in comparison with positron emission tomography/computed tomography in patients with neuroendocrine tumors. *Invest Radiol*. 2013;48:263–272.
21. Schiepers C, Dahlbom M. Molecular imaging in oncology: the acceptance of PET/CT and the emergence of MR/PET imaging. *Eur Radiol*. 2011;21:548–554.
22. Oberg K, Knigge U, Kwekkeboom D, et al. Neuroendocrine gastroenteropancreatic tumors: ESMO Clinical Practice Guidelines for diagnosis, treatment and follow-up. *Ann Oncol*. 2012;23(suppl 7):vii124–30.
23. Binderup T, Knigge U, Loft A, et al. Functional imaging of neuroendocrine tumors: a head-to-head comparison of somatostatin receptor scintigraphy, 123I-MIBG scintigraphy, and 18F-FDG PET. *J Nucl Med*. 2010;51:704–712.
24. Kayani I, Bomanji JB, Groves A, et al. Functional imaging of neuroendocrine tumors with combined PET/CT using 68Ga-DOTATATE (DOTA-DPhe1,Tyr3-octreotate) and 18F-FDG. *Cancer*. 2008;112:2447–2455.
25. Ambrosini V, Tomassetti P, Castellucci P, et al. Comparison between 68Ga-DOTA-NOC and 18F-DOPA PET for the detection of gastro-entero-pancreatic and lung neuro-endocrine tumours. *Eur J Nucl Med Mol Imaging*. 2008;35:1431–1438.
26. Breeman WA, de Jong M, de Blois E, et al. Radiolabelling DOTA-peptides with 68Ga. *Eur J Nucl Med Mol Imaging*. 2005;32:478–485.
27. Haug A, Auernhammer CJ, Wangler B, et al. Intraindividual comparison of 68Ga-DOTA-TATE and 18F-DOPA PET in patients with well-differentiated metastatic neuroendocrine tumours. *Eur J Nucl Med Mol Imaging*. 2009; 36:765–770.
28. Haug AR, Tiega Donfack BP, Trumm C, et al. 18F-FDG PET/CT predicts survival after radioembolization of hepatic metastases from breast cancer. *J Nucl Med*. 2012;53:371–377.
29. Fuccio C, Musto A, Cambioli S, et al. When should F-18 FDG PET/CT be used instead of 68Ga-DOTA-peptides to investigate metastatic neuroendocrine tumors? *Clin Nucl Med*. 2011;36:1109–1111.
30. Sourbron S, Ingrisch M, Siefert A, et al. Quantification of cerebral blood flow, cerebral blood volume, and blood-brain-barrier leakage with DCE-MRI. *Magn Reson Med*. 2009;62:205–217.
31. Makkat S, Luypaert R, Stadnik T, et al. Deconvolution-based dynamic contrast-enhanced MR imaging of breast tumors: correlation of tumor blood flow with human epidermal growth factor receptor 2 status and clinicopathologic findings—preliminary results. *Radiology*. 2008;249:471–482.
32. Do RK, Rusinek H, Taouli B. Dynamic contrast-enhanced MR imaging of the liver: current status and future directions. *Magn Reson Imaging Clin N Am*. 2009;17:339–349.
33. Ryeom HK, Kim SH, Kim JY, et al. Quantitative evaluation of liver function with MRI using Gd-EOB-DTPA. *Korean J Radiol*. 2004;5:231–239.
34. Nilsson H, Nordell A, Vargas R, et al. Assessment of hepatic extraction fraction and input relative blood flow using dynamic hepatocyte-specific contrast-enhanced MRI. *J Magn Reson Imaging*. 2009;29:1323–1331.
35. Haug AR, Auernhammer CJ, Wangler B, et al. 68Ga-DOTATATE PET/CT for the early prediction of response to somatostatin receptor-mediated radionuclide therapy in patients with well-differentiated neuroendocrine tumors. *J Nucl Med*. 2010;51:1349–1356.
36. Schwenzer NF, Schraml C, Muller M, et al. Pulmonary lesion assessment: comparison of whole-body hybrid MR/PET and PET/CT imaging—pilot study. *Radiology*. 2012;264:551–558.
37. Palmowski M, Schifferdecker I, Zwick S, et al. Tumor perfusion assessed by dynamic contrast-enhanced MRI correlates to the grading of renal cell carcinoma: initial results. *Eur J Radiol*. 2010;74:e176–80.
38. Thierbach R, Schulz TJ, Isken F, et al. Targeted disruption of hepatic frataxin expression causes impaired mitochondrial function, decreased life span and tumor growth in mice. *Hum Mol Genet*. 2005;14:3857–3864.
39. Warburg O. On the origin of cancer cells. *Science*. 1956;123:309–314.
40. Warburg O, Wind F, Negelein E. The metabolism of tumors in the body. *J Gen Physiol*. 1927;8:519–530.
41. Rossignol R, Gilkerson R, Aggeler R, et al. Energy substrate modulates mitochondrial structure and oxidative capacity in cancer cells. *Cancer Res*. 2004; 64:985–993.
42. Rustin P. Mitochondria, from cell death to proliferation. *Nat Genet*. 2002; 30:352–353.
43. Cyran CC, Sourbron S, Bochmann K, et al. Quantification of supra-aortic arterial wall inflammation in patients with arteritis using high resolution dynamic contrast-enhanced magnetic resonance imaging: initial results in correlation to [18F]-FDG PET/CT. *Invest Radiol*. 2011;46:594–599.
44. Haug AR, Rominger A, Mustafa M, et al. Treatment with octreotide does not reduce tumor uptake of (68)Ga-DOTATATE as measured by PET/CT in patients with neuroendocrine tumors. *J Nucl Med*. 2011;52:1679–1683.

6. Publikation II:

Diagnostic Accuracy of Dynamic Gadoxetic-Acid Enhanced MRI and PET/CT Compared in Patients With Liver Metastases From Neuroendocrine Neoplasms

Original Research

Diagnostic Accuracy of Dynamic Gadoxetic-Acid–Enhanced MRI and PET/CT Compared in Patients With Liver Metastases From Neuroendocrine Neoplasms

Marco Armbruster,[1] Christoph J. Zech, MD,[1,2] Steven Sourbron, PhD,[3] Felix Ceelen,[1] Christoph J. Auernhammer, MD,[4] Carsten Rist, MD,[1] Alexander Haug,[5] Amit Singnurkar, MD,[6] Maximilian F. Reiser, MD,[1] and Wieland H. Sommer, MD[1]*

Purpose: To evaluate the diagnostic accuracy of dynamic-contrast–enhanced (DCE) MRI in comparison to both ^{18}F-FDG- and ^{68}Ga-DOTATATE-PET/CT in patients with liver metastases of neuroendocrine neoplasms (NEN).

Materials and Methods: Thirty-two patients with hepatic metastases from NEN were examined both in DCE-MRI and positron emission tomography/computed tomography (PET/CT), using either ^{18}F-fluorodeoxyglucose (^{18}F-FDG) or ^{68}Ga-DOTATATE as tracer. DCE-MRI was performed at 3 Tesla with Gd-EOB-DTPA acquiring 48 slices every 2.2 s for 5 min. Three regions of interest (ROIs) representing liver background and liver metastases were defined in fat-saturated T1w three-dimensional GRE MRI sequences in the hepatobiliary phase. Corresponding ROIs were then defined in the DCE-MRI- and in the PET/CT-dataset. Area under the curve (AUC) was calculated for the differentiation between metastases and liver background for DCE-MRI and PET-CT parameters.

Results: AUC was very high for SUV_{mean} (mean standardized uptake value) derived from ^{68}Ga-DOTATATE- (AUC = 0.966), and ^{18}F-FDG-PET/CT (AUC = 0.989). For DCE-MRI parameters, arterial flow fraction and intracellular uptake fraction showed the highest AUCs (AUC = 0.826, AUC = 0.819, respectively). The combination of those two had an AUC of 0.949. The combination of DCE-MRI and PET-CT parameters resulted in the highest AUC.

Conclusion: Both PET/CT parameters and DCE-MRI perfusion parameters show a high diagnostic accuracy in the distinction between liver metastases and liver tissue. Our data suggest that both modalities provide complementary information.

Key Words: DCE-MRI; PET/CT; diagnostic accuracy; neuroendocrine tumor; liver metastases
J. Magn. Reson. Imaging 2014;40:457–466.

NEUROENDOCRINE NEOPLASMS (NENs) of the gastro-entero-pancreatic system constitute a very heterogeneous group of malignancies with an increasing incidence during the last few years (1). Given that a large number of these neoplasms do not demonstrate hormone secretion or manifest with clinical symptoms, many patients have advanced stage disease with distant metastases at the time of diagnosis (2). The liver is the most common site of metastatic disease, and hepatic tumor load is associated with high morbidity and mortality (3). Recent studies reveal that hepatic tumor load plays an important role in the therapeutic work-up and the prediction of therapeutic outcome (4,5). As a consequence, assessing hepatic tumor load is not only necessary in initial staging of NENs, but also for treatment monitoring in follow-up examinations.

Nevertheless, it remains challenging on the one hand to quantify the tumor burden and on the other hand to distinguish metastatic from normal liver tissue, especially in disseminated metastatic infiltration. Therefore, different imaging modalities currently coexist, including established modalities like contrast-enhanced computed tomography (CT) and MRI, as

[1]Department of Clinical Radiology, University Hospitals-Grosshadern, Ludwig-Maximilians University, Munich, Germany.
[2]Clinic of Radiology and Nuclear Medicine, University Hospital Basel, Basel, Switzerland.
[3]Division of Medical Physics, University of Leeds, Leeds, United Kingdom.
[4]Department of Internal Medicine II, Campus Grosshadern, Interdisciplinary Center of Neuroendocrine Tumors of the GastroEntero-Pancreatic System (GEPNET-KUM), University Hospitals-Grosshadern, Ludwig-Maximilians University, Munich, Germany.
[5]Department of Nuclear Medicine, University Hospitals-Grosshadern, Ludwig-Maximilians University, Munich, Germany.
[6]Department of Nuclear Medicine, McMaster University, Hamilton, Canada.
*Address reprint requests to: W.H.S., Department of Clinical Radiology, University of Munich, Grosshadern Campus, Marchioninistr 15, 81377 Munich, Germany. E-mail: wieland.sommer@med.uni-muenchen.de
Received March 5, 2013; Accepted August 5, 2013.
DOI 10.1002/jmri.24363
View this article online at wileyonlinelibrary.com.

well as functional imaging modalities, especially positron emission tomography (PET)/CT with different radiotracers.

For MRI, several metastasis-specific imaging parameters for NENs have been described, including hyperintense signal intensity (SI) on fluid-fluid levels on T2-weighted (T2w) imaging and arterial hypervascularity (6–8). Recent studies also suggest diffusion-weighted (DW) MR sequences to be very sensitive for the detection and characterization of liver metastases from NEN and particularly help identifying small lesions (9,10). Furthermore, the introduction of gadolinium-ethoxybenzyl-diethylenetriamine penta-acetic acid (Gd-EOB-DTPA, Primovist®, Bayer Healthcare) in MRI examinations of the liver has increased sensitivity and specificity for the detection of liver metastases. Gd-EOB-DTPA-MRI is currently regarded as the standard of reference for detection of liver metastases and the evaluation of tumor load in the liver (11–13). However, disseminated metastatic infiltration may be also challenging for this approach.

In addition to morphologic assessment PET/CT provides information regarding metabolic activity or receptor status of the tumor, depending on the radiotracer. Amongst these tracers, two have emerged as suitable for the detection and discrimination of liver metastases from neuroendocrine neoplasms (NENLMs): While ^{18}F-fluorodeoxyglucose (^{18}F-FDG) was found to visualize tumor metabolism better in poorly differentiated NENs with high proliferation indices, the somatostatin analogue ^{68}Ga-DOTATATE / ^{68}Ga-DOTATOC seems to be better suited for the detection of well-differentiated tumors (14).

For functional MRI approaches, particularly dynamic-contrast–enhanced MRI (DCE-MRI) of the liver emerged promising to deliver further information for the evaluation of metastatic stage disease NEN. Given that DCE-MRI is capable of quantifying the microcirculatory status of the liver (15–17) it has the potential to go beyond the morphologic limitations of contrast-enhanced MRI and provide regional and global information about hepatic blood flow and liver function (16,18). For this purpose especially the hepatocyte-specific contrast agent Gd-EOB-DTPA seems to be suitable, as it distributes to all anatomical structures of the liver and therefore allows to obtain not only detailed morphological assessment in the hepatobiliary phase with fat-saturated T1w three-dimensional (3D) GRE sequences but also the full range of flow- and uptake-related perfusion parameters in only one comprehensive MR examination and with only one application of a standard dose of contrast agent (13,17,19). However, according to our knowledge, there are only a few reports on the value of DCE-MRI parameters for assessment of distant stage disease NEN and little is known about which parameters are best suited to differentiate between the liver background and metastatic tissue.

Therefore, the aim of the current study was to evaluate the diagnostic accuracy of perfusion parameters derived from dynamic Gd-EOB-DTPA–enhanced MRI in comparison to standardized uptake values (SUVs) derived from PET/CT imaging for the differentiation between liver background tissue and liver lesions in patients with proven metastases from neuroendocrine tumors. Among others, the question to be addressed was if the combination of DCE-MRI and PET/CT may have additional value and provide complementary information.

MATERIAL AND METHODS

Clinical Data

This was a prospective, single-institution study conducted between December 2008 and April 2012. The local institutional review board approved the study and informed consent was obtained from all patients before the examinations. The study cohort consisted of 47 patients with mean age 59.7 ± 10.2 (range, 42–82 years) and a female-to-male ratio of 24/23.

Histopathologic Assessment

The diagnosis of NEN was confirmed histopathologically in all cases. If the origin of the primary tumor site was known, histological diagnosis was provided by resection or biopsy of the primary tumor. For patients with unknown origin tissue was obtained by biopsy of liver metastases. Furthermore, in those patients who received the resection or biopsy in our tertiary center we also obtained Ki-67 labeling index to assess tumor grading.

Diagnostic Imaging

All patients received a MRI scan of the liver that was scheduled as a regular follow-up examination for imaging surveillance, which is routinely performed every 3 months in our tertiary center for neuroendocrine neoplasms to assess the exact tumor burden of the liver. Furthermore, for assessment of other distant metastases all patients underwent whole-body PET/CT imaging as part of their routine follow-up imaging, either using ^{18}F-FDG or ^{68}Ga-DOTATATE.

In most cases, DCE-MRI- and PET/CT-datasets were acquired within 24h ($n = 33$ of 47). All examinations with a date difference greater than 14 days have been excluded from this study.

Patients' hematocrit values were recorded on the day of the DCE-MRI examination. Fifteen of the patients had more than one follow-up examination. Additional examinations of these patients were excluded.

DCE-MRI

Patients were imaged at 3T (Magnetom Verio, Siemens Healthcare, Erlangen, Germany), using a 32-channel phased array body- and spine coil. Our standard liver-MRI protocol consisted of precontrast sequences including in- and opposed phased T1-weighted imaging and various postcontrast sequences, including T2-weighted imaging, coronal and transverse T1-weighted 3D gradient recalled echo (GRE) imaging with fat-saturation 20 min after contrast injection. DCE-MRI data of the whole liver were acquired for 5 min at a temporal resolution of 2.2 s, using a 3D T1-

weighted spoiled gradient-echo sequence that was accelerated using view sharing and parallel imaging (TWIST). Imaging parameters were: 48 coronal slices (4 mm), pixel size 2.1 mm, flip angle 15°, TR: 2.37 ms, TE: 0.83 ms, phase/slice oversampling 17%/25%, 400 mm field-of-view, 100% phase field-of-view, 192x192 matrix, phase/slice resolution 100%/63%, partial Fourier 7/8, central region A 20%, sampling density B 25%, GRAPPA factor 4 with 24 reference lines. The contrast agent Gd-EOB-DTPA (Primovist®, Bayer Healthcare, Germany) was injected at a dose of 0.1 mL/kg with a flow rate of 2 mL/s, 10 s after starting the acquisition and flushed with 30 mL saline at the same rate. Patients were instructed to breathe shallowly during the acquisition.

PET/CT

Patients were examined either with ^{68}Ga-DOTATATE or ^{18}F-FDG, depending on the tumor grading and the tracer used in previous PET/CT examinations as described in the following section: If the examination was the first PET/CT examination of a patient ^{68}Ga-DOTATATE was used in tumors with low (G1; Ki67 $\leq$ 2%), intermediate (G2; 2% < Ki67 < 20%) or unknown proliferation indices (20), whereas ^{18}F-FDG was used in tumors with high proliferation (G3; Ki67 $\geq$ 20%) indices (21,22). In case that a patient received previous examinations, the previously used tracer was retained to provide for better follow-up interpretation.

^{68}Ga-DOTATATE was prepared as described previously (23,24). Whole-body PET scans were acquired in 3-dimensional mode with 3 min acquisitions per bed position using a Biograph 64 TruePoint PET/CT scanner (Siemens Healthcare, Erlangen, Germany). The emission sequence was started approximately 60 min after intravenous injection of 200 MBq of ^{68}Ga-DOTATATE or ^{18}F-FDG, similar to protocols used in other studies working with ^{68}Ga-labeled somatostatin analogs (23,25) or ^{18}F-FDG (26,27). Emission data were reconstructed with attenuation correction based on low-dose CT (20 mA, 140 kV, 512 × 512 matrix). All imaging was performed in combination with a diagnostic CT scan (100–190 mAs, depending on the region of the scanned organ; 120 kV; 2.5 mm collimation; pitch of 1.5) of the head, thorax, abdomen, and pelvis performed after a 2.5 mL/s intravenous injection of an iodinated contrast agent (Iomeprol 350 mg/mL, Bracco SpA, Milan, Italy; 1.5 mL/kg body weight). This scan was initiated 50 s postcontrast so as to depict the portal-venous phase of enhancement.

Postprocessing

DCE-MRI

All DCE-MRI data were postprocessed using the software PMI 0.4 (17,28,29). Contrast agent concentrations were approximated by the relative signal enhancement (30). The arterial input function (AIF) was defined inside the lumen of the abdominal aorta on a maximum enhancement map as follows: a radiologist with 5 years of experience in abdominal imaging and DCE-MRI broadly outlined the aorta above the renal arteries by drawing 3 or 4 ROIs on adjacent slices; the ROI was shrunk automatically by extracting the pixels in the top 10% of the value range. Arterial concentrations were corrected with the patient's hematocrit to derive plasma concentrations. Parametric maps of plasma flow and mean transit time were then calculated by deconvolving tissue concentrations with the AIF (19,29,31). To define the venous input function (VIF), both intra- and extrahepatic portions of the portal vein were defined on the plasma flow map on 3 or 4 adjacent slices. This ROI was shrunk by selecting the pixels in the top 10% of the value range (17). The complete 4-parameter dual-inlet two-compartment uptake model, with arterial delay correction, was fitted to all defined ROIs representing metastatic or background liver tissue (provided below). This model was used as it takes the special pharmacokinetic properties of the hepato-biliary contrast agent Gd-EOB-DTPA into account and has been recently validated for this purpose by Sourbron et al (17).

The following perfusion-parameters were calculated: arterial plasma flow (APF), venous plasma flow (VPF), total plasma flow (TPF), arterial flow fraction (AFF), extracellular volume (exVol), extracellular mean transit time (exMTT), intracellular uptake rate (UR) and hepatic uptake fraction (UF).

Definition of Regions of Interest

To account for intra-individual differences and to minimize the influence of outliers to calculated cutoff values three regions per patient representing the liver background and up to three viable metastases were identified on delayed coronal T1-weighted GRE sequences 20 min after contrast injection of Gd-EOB-DTPA. Information from diffusion weighted imaging, contrast-enhanced T1-weighted sequences and T2-weighted sequences were also taken into account to decide whether an area represents metastatic or normal liver tissue. Corresponding regions of interest (ROIs) were defined accordingly on coronal PET/CT datasets and DCE-MRI semiparametric maps. For ROIs representing metastatic tissue the entire lesion was included. In case of central necrosis, only the viable rim was included into the analysis.

The co-registration of the morphological sequence with both PET/CT and DCE-MRI was performed using anatomical landmarks and distances from the ROI to the anatomical landmarks, standardized by the following procedure: The origin of the renal arteries was defined in the morphologic sequence, in DCE-MRI MTT-map and PET/CT. Corresponding distances in x, y and z direction from the anatomical landmark to the estimated position of the ROI were calculated using DICOM-header information (slice-thickness and slice-margin). According to the calculated position and to direct visual correlation with the morphological sequences corresponding ROIs were defined both in DCE-MRI MTT-map and PET/CT.

Statistical Analysis

Statistical analysis was performed by using commercially available software (SAS 9.3, SAS Institute Inc.,

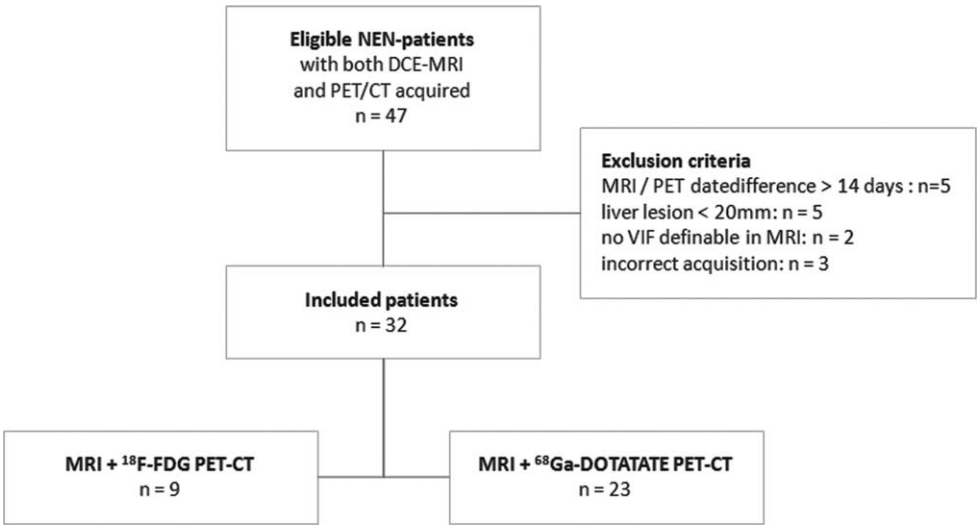

Figure 1. Flowchart of study profile.

Cary, NC). To confirm that continuous variables were normally distributed, the Kolmogorov-Smirnov test was applied. Normal distribution was evaluated for SUV, APF, VPF, TPF, AFF, exVol, exMTT, UR, and UF. Variables following normal distribution are reported as means ± standard deviations. To examine whether normally distributed variables were different between metastases and liver background, the Student's t-test for independent samples was applied to test for differences in means. In case of nonnormal distribution, the Wilcoxon rank sum test was used. Receiver operating characteristic (ROC) curves were plotted using SAS software and the following SAS macros: SAS ROC (version 1.7) and ROCPLOT (version 1.1). Level of significance α was 0.05, resulting in 95% confidence intervals (CIs). Areas under the curves (AUCs) were calculated. Optimal cut off values were estimated by maximizing total accuracy using univariate logistic regression analysis.

In a multivariable logistic regression model we tested for incremental values of using more than one perfusion parameters. In the first multivariate logistic regression model, all DCE-MRI parameters were added and a forward stepwise selection algorithm with a *P* value of 0.05 was used for entering and removing predictors to or from the model. In two additional multivariate models, the hypothesis was tested, if the combination of SUV and DCE-MRI parameters further increases the area under the ROC curve. Because SUV values of ^{68}Ga-DOTATATE and of ^{18}F-FDG were mutually exclusive in that there were no patients who received two PET/CTs with different tracers, we performed the analysis separately for each tracer. The same inclusion and exclusion parameters were used as for the previous model and a forward selection algorithm was chosen. To account for overfitting of the multivariate logistic regression analysis models, we validated the three models by bootstrapping and 1000 iterations of the models. The corrected AUC values were calculated using the SAS Macro "OPTIMISM Bootstrap Estimate" developed by Shimon Shaykevich, from the Clinical Effectiveness Harvard School of Public Health. This Macro was also used to calculate the standard deviation for the corrected AUC.

RESULTS

Patients

Fifteen of 47 DCE-MRI examinations were excluded from the analysis because the date-difference between DCE-MRI and PET/CT was greater than 14 days (n = 5), no lesions with diameters greater than 20 mm could be defined either on PET/CT or DCE-MRI images (n = 5), the venous input function (VIF) could not be clearly identified (n = 2) or acquisition and postprocessing of data was not possible due to strong motion artifacts (n = 2) or delayed start of DCE-MRI sequence (n = 1). Among the 32 remaining examinations there were 23 examinations with ^{68}Ga-DOTATATE and 9 examinations with ^{18}F-FDG as used PET-tracer (see Fig. 1).

The primary tumor site of the NEN was the colon (n = 11), pancreas (n = 10), ileum (n = 9), jejunum (n = 6) and the stomach (n = 4). The tumor was of unknown origin in 7 individuals. Most of the patients had multiple previous treatments: Transarterial radioembolization using ^{90}Yttrium (n = 24), somatostatin analogue therapy with ocreotide or lanreotide (n = 16), peptide receptor radionuclide therapy using ^{177}Lutetium-DOTATATE and ^{90}Yttrium-DOTATATE (n = 16), chemotherapy (n = 12), hemihepatectomy (n = 8), transarterial chemoembolization (n = 4) or radiofrequency ablation (n = 3) (see Table 1).

ROI Definitions

A total of 74 metastases and 96 ROIs within normal-appearing liver tissue representing liver background were defined in morphological MRI sequences, DCE-MRI, and PET/CT datasets (see Fig. 2). Mean diameter of all liver lesions was 49.19 ± 28.86 mm.

Mean number of target metastases (2.34, 2.22, respectively) and mean diameter of target metastases (47.64 ± 27.5 mm, 52.84 ± 32.05 mm, respectively) were similar ($P = 0.7038$; $P = 0.5148$, respectively) between the ^{68}Ga-DOTATATE- and the ^{18}F-FDG-group.

Table 1
Patient and Clinical Characteristics of Study Cohort (n = 47)*

Characteristic	N
Sex	
Male	23
Female	24
Primary tumor site	
Colon	11
Pancreas	10
Ileum	9
Jejunum	6
Stomach	4
Unknown	7
Histopathologic tumor grading	
G1 (Ki67 <= 2%)	4
G2 (2% < Ki67 < 20%)	7
G3 (Ki67 >= 20%)	5
Unkown	31
Previous therapies	
TARE (^{90}Yttrium)	24
Somatostatinanaloga therapy	16
PRRT (^{117}Lutetium + ^{90}Yttrium)	16
Chemotherapy	12
Hemihepatectomy	8
TACE	4
RFA	3

*Mean age ± SD was 59.8 ± 10.5 y (age range: 42–82 yr).
TARE = transarterial radioembolization; PRRT = peptide receptor radionuclide therapy; TACE = transarterial chemoembolization; RFA = radiofrequency ablation.

Differentiation Between Metastases and Liver Background

Table 2 shows average values of all measured PET/CT and DCE-MRI parameters both for metastatic and normal-appearing liver tissue as well as estimated cutoff values.

^{68}Ga-DOTATATE PET/CT

SUV_{mean} from ^{68}Ga-DOTATATE PET/CT was significantly higher for metastases (18.1 ± 8.7; n = 53) than for liver background (5.0 ± 1.5) ($P < 0.0001$). A cutoff value was calculated as 7.9 (Sensitivity: 92.6%, Specificity: 93.8%) (see Table 2). AUC of SUV_{mean} was estimated at 0.966 (see Fig. 3).

^{18}F-FDG PET/CT

SUV_{mean} from ^{18}F-FDG-PET CT was also higher for liver-metastases (10.3 ± 5.3; n = 21) than for ROIs of normal-appearing liver tissue (2.2 ± 0.7) ($P < 0.0001$). The optimal cutoff value which was calculated for our dataset was 3.9 (Sensitivity: 95.0%, Specificity: 91.3%) (see Table 2). AUC of SUV_{mean} was measured as 0.989 (see Fig. 3).

DCE-MRI Parameters

Plasma Flow

Metastases showed a significantly higher APF (61.3 ± 56.2 mL/min/100 mL; n = 74), compared with nonmetastatic liver tissue (20.4 ± 15.2 mL/min/100 mL) ($P < 0.0001$), while VPF rates were significantly lower for metastases (12.9 ± 31.1 mL/min/100 mL; n = 74) than for the liver background (30.6 ± 30.4 mL/min/100 mL) ($P < 0.0001$). Cutoff values for APF and VPF were 26.0 mL/min/100 mL (Sensitivity: 91.9%; Specificity: 77.3%), 6.9 mL/min/100 mL (Sensitivity: 73.0%; Specificity: 73.3%), respectively. ROC-analysis resulted in AUCs of 0.901, 0.763, respectively. The total plasma flow (APF + VPF) was increased up to 44% in metastases (73.2 ± 79.7 mL/min/100 mL; n = 74) compared with the liver background (50.9 ± 28.5 mL/min/100 mL)($P = 0.0018$) (see Table 2). Optimal cutoff value for the TPF was calculated at 39.1 mL/min/100 mL (Sensitivity: 85.1%; Specificity: 44.3%), while AUC was estimated at 0.645. The AFF, too, was significantly higher in metastases (87.7 ± 21.5%) than in ROIs representing nonmetastatic liver tissue (48.2 ± 31.9%) ($P < 0.0001$) and showed highest sensitivity (83.8%) and specificity (76.1%) for a cutoff value of 71.8%. The AUC for the arterial flow fraction was 0.826.

Extracellular Volume and Extracellular Mean Transit Time

Mean exVol was significantly higher for lesions (18.5 ± 8.3 mL/100 mL; n = 74) than for ROIs representing liver background (14.0 ± 8.3 mL/100 mL) ($P < 0.0001$), while the exMTT did not differ significantly (18.8 ± 7.2 s; n = 74 versus 17.7 ± 9.7 s) ($P = 0.2196$) (see Table 2). AUC of exVol was 0.716 and the cutoff value was 17.9 mL/100 mL (Sensitivity: 51.4%; Specificity: 89.8%).

Intracellular Uptake Rate and Uptake Fraction of Contrast Agent

The intracellular uptake rate of Gd-EOB-DTPA was significantly different between metastases and liver background ($P < 0.0001$) and was significantly lower for metastases (1.4 ± 1.2 /100 mL/min; n = 74) than for nonmetastatic liver tissue ROIs (3.4 ± 2.1 /100 mL/min). Also the hepatic uptake fraction of Gd-EOB-DTPA was significantly lower for metastases (2.5 ± 1.9%; n = 74) than for the liver background (7.7 ± 5.4%) ($P < 0.0001$) (see Table 2). Cutoff values for uptake rate and uptake fraction were calculated at 2.5 /100/min (Sensitivity: 90.5%; Specificity: 64.8%), 4.1% (Sensitivity: 83.8%; Specificity: 70.5%), respectively. ROC-curve of these parameters showed an AUC of 0.797, 0.819, respectively.

Multivariate Logistic Regression Analysis

Model 1: DCE-MRI Parameters

The model selected the AFF as the strongest predictor (adjusted odds ratio [aOR]: 1.060; 95% CI: 1.040–1.079), followed by the UF (aOR: 0.567; 95% CI: 0.453–0.708). The AUC increased by the addition of a second factor from 0.826 to 0.949 (see Fig. 4). After application of bootstrapping, the degree of optimism for the AUC was calculated as 0.001. The corrected and validated value for the AUC for the two-factor regression model using AFF and UF as predictors was 0.948 ± 0.018.

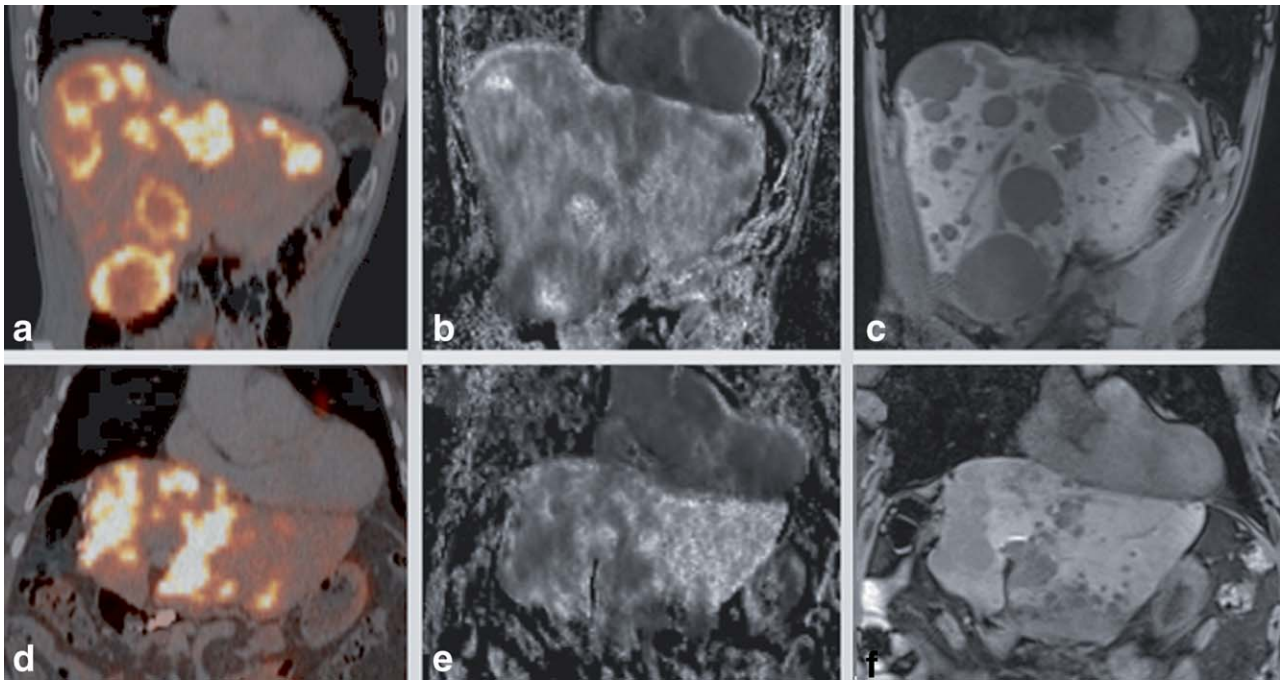

Figure 2. Metastatic liver tissue in patients suffering from neuroendocrine neoplasms. **a–c:** Coronal images through the fused images of the PET/CT (**a**), the mean transit time semiparametric map of the corresponding DCE-MRI dataset (**b**) and T1w 3D GRE sequence in the hepato-biliary phase (20 min post contrast injection) (**c**) in a 70-year-old man with multiple metastases. The tracer used in this PET/CT examination was ^{68}Ga-DOTATATE. **d–f:** Coronal images through the fused images of the PET/CT (**d**), the mean transit time semiparametric map of the corresponding DCE-MRI dataset (**e**) and T1w 3D GRE sequence in the hepato-biliary phase (**f**) in a 66-year-old man with disseminated hepatic metastases. The tracer used in this PET/CT examination was ^{18}F-FDG. A visual comparison between the PET/CT and the MTT-semiparametric map also indicates a good visual correlation between DCE-MRI and PET/CT with both radiotracers to differentiate between lesions and liver background. The images in the hepato-biliary phase allow for a precise evaluation of morphological information such as lesion size and identification of small satellite metastases.

Model 2: DCE-MRI and ^{18}F-FDG PET/CT

For the combination of SUV from ^{18}F-FDG PET/CT and DCE-MRI parameters, a model building was not possible due to a complete separation of data points after entering the first variable APF. This is probably due to the small sample size.

Model 3: DCE-MRI and ^{68}Ga-DOTATATE PET/CT

For the combination of SUV from ^{68}Ga-DOTATATE PET/CT and DCE-MRI parameters, the final multivariate logistic regression model resulted in a three factor model containing SUV, APF, and UF. The following estimates were obtained by the model: (aOR: 1.086; 95% CI: 1.005–1.172), UF (aOR: 0.559; 95% CI: 0.299–1.047), $SUV_{GaDOTATATE}$ (aOR: 9.915; 95% CI: 1.269–77.446). The AUC of the one factor model containing SUV increased by the addition of the DCE-MRI factor APF from 0.967 to 0.992. The addition of the third factor UF increased the AUC slightly to 0.996. After application of bootstrapping, the degree of optimism for the AUC was calculated as 0.004. The corrected and validated value for the AUC for the three-factor regression model using $SUV_{GADOTATATE}$, APF and UF as predictors was 0.992 ± 0.004.

Table 2
Diagnostic Accuracy of DCE-MRI and PET/CT*

		Metastases	Liver-background	*P* Value	Cutoff	Sensitivity	Specificity
PETCT	SUV_{mean} (^{68}Ga-DOTATATE)	18.1 ± 8.7; n=53	5.0 ± 1.5; n=69	<0.0001	7.9	92.6%	93.8%
	SUV_{mean} (^{18}F-FDG)	10.3 ± 5.3; n=21	2.2 ± 0.7; n=27	<0.0001	3.9	95.0%	91.3%
DCE-MRI	APF (ml/min/100ml)	61.3 ± 56.2; n=74	20.4 ± 15.2; n=96	<0.0001	26.0	91.9%	77.3%
	VPF (ml/min/100ml)	12.9 ± 31.1; n=74	30.6 ± 30.4; n=96	<0.0001	6.9	73.0%	73.3%
	TPF (ml/min/100ml)	73.2 ± 79.7; n=74	50.9 ± 28.5; n=96	0.0018	39.1	85.1%	44.3%
	Arterial flow fraction (%)	87.7 ± 21.5; n=74	48.2 ± 31.9; n=96	<0.0001	71.8	83.8%	76.1%
	Extracellular vol. (ml/100ml)	18.5 ± 8.3; n=74	14.0 ± 8.3; n=96	<0.0001	17.9	51.4%	89.8%
	Extracellular MTT (sec)	18.8 ± 7.2; n=74	17.7 ± 9.7; n=96	0.2196	–	–	–
	Uptake rate (/100/min)	1.4 ± 1.2; n=74	3.4 ± 2.1; n=96	<0.0001	2.5	90.5%	64.8%
	Uptake fraction (%)	2.5 ± 1.9; n=74	7.7 ± 5.4; n=96	<0.0001	4.1	83.8%	70.5%

*Wilcoxon rank sum test analysis for testing differences in means. If significant: cutoff values with corresponding sensitivity and specificity.

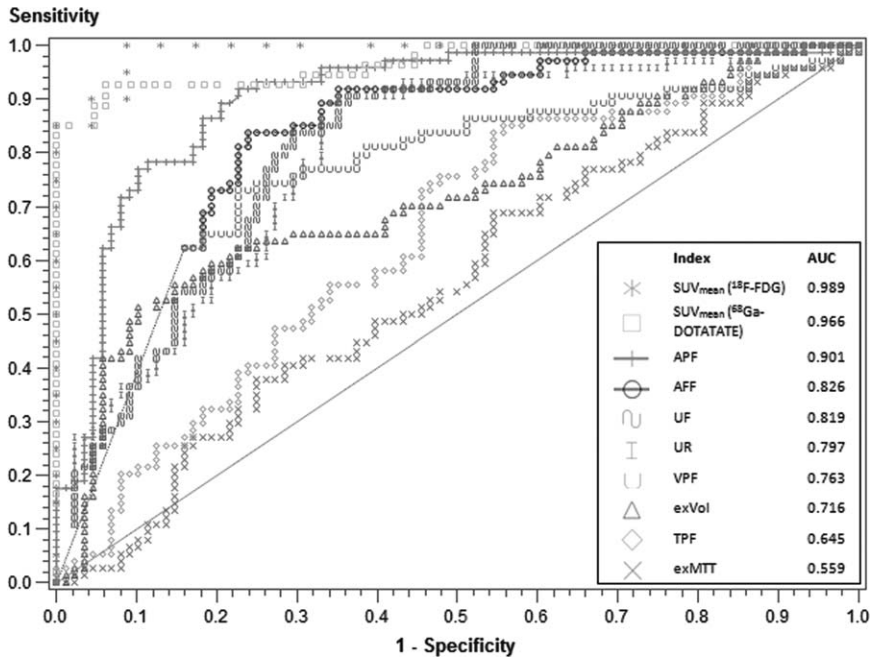

Figure 3. ROC curve and area under the curve of both SUV_{mean} derived from PET/CT and DCE-MRI parameters. The true-positive rate (y axis: sensitivity) is plotted against the false-positive rate (x axis: 1-specificity).

DISCUSSION

In the current study, we analyzed the diagnostic performance of DCE-MRI parameters to differentiate between metastases and liver tissue in comparison to SUVs derived from PET/CT using two different radiotracers. Similarly to other studies, we could show that SUVs derived from PET/CT using ^{68}Ga-DOTATATE and ^{18}F-FDG, as well as several perfusion parameters derived from DCE-MRI differed significantly between normal liver tissue and hepatic lesions (15,17,32,33). Furthermore, we determined cutoff values for both SUVs and perfusion-parameters to estimate sensitivity and specificity: Standardized uptake values from both ^{68}Ga-DOTATATE- and ^{18}F-FDG-PET/CT as well as arterial plasma flow, arterial flow fraction, intracellular uptake rate, and hepatic uptake fraction from DCE-MRI with Gd-EOB-DTPA showed a comparatively high diagnostic accuracy and correspondingly relative high areas under the ROC-curve.

Especially flow-related parameters (APF, VPF, and AFF) as well as uptake-related parameters (UR, UF) emerged as promising markers to differentiate between metastatic and nonmetastatic liver tissue from our study. The multivariate regression analysis also showed that parameters from the two groups (flow and uptake related parameters) provide complementary information leading to an even higher diagnostic accuracy with an area under the ROC curve around 0.95. Furthermore, we could show that these parameters also increase the diagnostic accuracy of PET/CT when used in combination with the SUV.

Regarding the generalizability of our results of the predictive value of DCE-MRI parameters, these findings must be discussed in the context of the primary tumor of the liver metastases. Neuroendocrine neoplasms are known to be highly vascularized (34,35) which makes flow-related parameters suitable biomarkers. This has yet to be shown for liver metastases of non-neuroendocrine origin which are less vascularized. For parameters related to the uptake of Gd-EOB-DTPA, the ability to discriminate between metastases and liver background should be less influenced by the origin of the liver metastases. The uptake of Gd-EOB-DTPA into the hepatocytes occurs by means of the organic anion transporter polypeptides (OATP1B1 and B3). They are only present on the sinusoidal membrane of hepatocytes and make the uptake specific for hepatocytes (36). These

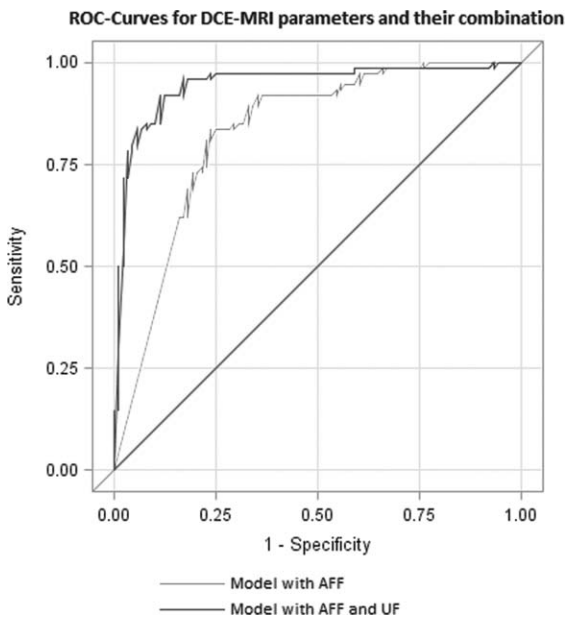

Figure 4. Increase in the area under the ROC curve when using two DCE-MRI parameters as predictors. In step 1, AFF was entered into the model, leading to an AUC of 0.8262. In step 2, uptake fraction of Gd-EOB-DTPA (UF) was entered into the model and the AUC increased to 0.949.

characteristics cause Gd-EOB-DTPA to behave similarly to nonspecific gadolinium-based contrast agents during the dynamic phases and to add additional information during subsequent phases, improving the detection and characterization of focal liver lesions (12). Although one would not expect OATP1B1/3 on metastases, we found a measurable uptake rate and uptake fraction of Gd-EOB-DTPA even in liver metastases. This is in line with previously published data and can be explained by distribution of the contrast agent into the interstitial compartment of tumors (12). Because the wash-out of the interstitial compartment is much faster than the biliary excretion from the hepatocytes by means of the multidrug resistance-associated proteins MRP2 at the canalicular membrane, a longer acquisition time might be able to differentiate between true intracellular hepatocyte uptake and the interstitial tumor uptake and possibly lead to an increased ability to differentiate between these two types of tissue.

The current study revealed the DCE-MRI parameter extracellular volume to be significantly different between metastatic and background liver tissue with respect to its mean values, but to have a poor diagnostic accuracy when differentiating between these two entities. Nevertheless this parameter might be useful for a different objective. A recent study with 29 patients reported that the distribution volume measured by DCE-MRI is associated with treatment response to ^{90}Y-DOTATOC (37). Consequently, changes to the extracellular volume representing a distribution volume parameter might possibly be rather suitable for therapy monitoring than for lesions' diagnosis. Further studies are required to work out the predictive value not only of distribution-related parameters like extra- and intracellular volume, but also of flow- and uptake-related parameters of DCE-MRI in the growing diversity of treating NENLMs.

The results of our study also suggest that SUV_{mean} obtained on PET/CT can reliably differentiate between normal hepatic tissue and hepatic metastases when imaged with either ^{68}Ga-DOTATATE or ^{18}F-FDG, the choice of which depends on the degree of tumor differentiation. However, the findings on this study may have limited generalizability as only lesions over 2 cm in size were imaged. Specifically, detection rate of tumor can be limited due to partial volume effect when lesions are small (38), which reduces the sensitivity of PET/CT. This effect is independent of the imaging tracer used. We predict that smaller metastases, particularly lesions less than 1 cm in size, would result in a lower sensitivity for both tracers.

In a study with 22 patients by Schreiter et al. which included metastases measuring less than 1 cm, there was a lower diagnostic accuracy with ^{68}Ga-DOTATATE-PET/CT (Sensitivity: 73.5%; Specificity: 88.2%) (39). Also, the use of firm cutoffs in the characterization of tumor tissue on PET/CT can be limited due to the inherent variability of the SUV measurement which may vary with tracer uptake time, body mass index, administered dose, imaging device, and reconstruction algorithm. In the case of ^{18}F-FDG-PET/CT, SUV may be underestimated due to high serum glucose level. For ^{68}Ga-DOTATATE-PET/CT, a falsely low SUV may be obtained if the patient is undergoing somatostatin-analogue therapy. Finally, there is a significant selection bias in our study for identifying tracer avid metastases because the PET/CT examinations were in large part follow-up examinations with proven uptake on previous studies.

In the current discussion on MR-PET, a combination of PET information and morphological MRI-sequences with hepatocyte-specific contrast agent seems to lead to an optimal diagnostic and functional evaluation of patients with liver metastases of neuroendocrine neoplasms (32,39). Although we found a very high diagnostic accuracy both for ^{68}Ga-DOTATATE and ^{18}F-FDG for liver metastases, Gd-EOB-DTPA–enhanced MRI of the liver offers advantages in the assessment of micrometastases and the determination of tumor burden in the liver (13,40). Especially for disseminated metastatic infiltration, it remains challenging to confirm suspected tissue as clearly metastatic. In these cases, DCE-MRI parameters, particularly high rates of arterial plasma flow and a high arterial flow fraction as well as a low intracellular uptake rate of contrast agent may be useful to increase specificity and potentially help identifying remaining viable tumor after treatment. In view of the current trend toward hybrid imaging techniques, particularly MR-PET, the combination of morphological MRI-sequences, DCE-MRI-, and PET- parameters may increase the total diagnostic accuracy and guide optimal therapy.

Given that in the current study complete data from all three imaging modalities (MR, DCE-MRI, and PET/CT) were only assessed once per patient, we were not able to correlate the functional parameters from DCE-MRI and PET/CT to morphologic tumor response criteria like, eg, the commonly used response evaluation criteria in solid tumors (RECIST). Further studies with a different study design and multiple follow-ups are needed to investigate this correlation and to determine the value of DCE-MRI parameters in the evaluation of treatment response.

These data must also be interpreted in the context of the study design. Although the diagnosis of NEN was confirmed in all patients histopathologically, we used the morphological MRI-sequence of hepatocyte-specific contrast agent late liver phase and tissue appearance on T2-weighted images as gold standard for ROI-definition of liver metastases. Given that liver metastases from NENs can show diffuse organ involvement, the difference between metastatic and nonmetastatic tissue is not always possible. Nevertheless, we tried to avoid any misclassification by correlation with all available morphological sequences. As discussed above, we used a cutoff value of 2 cm for liver metastases, mainly to mitigate limitations related to diaphragmatic motion resulting from the gentle breathing of patients during the 5-min acquisition period of DCE-MRI. The parameter estimates for diagnostic performance may therefore be lower in smaller metastases and the reported diagnostic accuracy might not be generalized for all lesions. Cutoff values

may be corrected in future studies if motion artifacts can be minimized by sequence optimization and image restriction.

In conclusion, we could show that perfusion parameters derived from DCE-MRI and standardized uptake values from PET-imaging provide important functional information for liver metastases of neuroendocrine tumors. These parameters may be helpful to distinguish between metastatic and nonmetastatic tissue and therefore have the potential to increase diagnostic sensitivity and specificity when used in combination with other imaging modalities.

ACKNOWLEDGMENTS

We thank Fran Cook and Shimon Shaykevich, Harvard School of Public Health, for their helpful comments on the statistical analysis.

REFERENCES

1. Ramage JK, Ahmed A, Ardill J, et al. Guidelines for the management of gastroenteropancreatic neuroendocrine (including carcinoid) tumours (NETs). Gut 2012;61:6–32.
2. Auernhammer CJ, Goke B. Therapeutic strategies for advanced neuroendocrine carcinomas of jejunum/ileum and pancreatic origin. Gut 2011;60:1009–1021.
3. Yao JC, Hassan M, Phan A, et al. One hundred years after "carcinoid": epidemiology of and prognostic factors for neuroendocrine tumors in 35,825 cases in the United States. J Clin Oncol 2008;26:3063–3072.
4. Cao CQ, Yan TD, Bester L, Liauw W, Morris DL. Radioembolization with yttrium microspheres for neuroendocrine tumour liver metastases. Br J Surg 2010;97:537–543.
5. Dunfee BL, Riaz A, Lewandowski RJ, et al. Yttrium-90 radioembolization for liver malignancies: prognostic factors associated with survival. J Vasc Interv Radiol 2010;21:90–95.
6. Debray MP, Geoffroy O, Laissy JP, et al. Imaging appearances of metastases from neuroendocrine tumours of the pancreas. Br J Radiol 2001;74:1065–1070.
7. Dromain C, de Baere T, Baudin E, et al. MR imaging of hepatic metastases caused by neuroendocrine tumors: comparing four techniques. AJR Am J Roentgenol 2003;180:121–128.
8. Sommer WH, Zech CJ, Bamberg F, et al. Fluid-fluid level in hepatic metastases: a characteristic sign of metastases of neuroendocrine origin. Eur J Radiol 2012;81:2127–2132.
9. d'Assignies G, Fina P, Bruno O, et al. High sensitivity of diffusion-weighted MR imaging for the detection of liver metastases from neuroendocrine tumors: comparison with T2-weighted and dynamic gadolinium-enhanced MR imaging. Radiology 2013;268: 390–399.
10. Sankowski AJ, Cwikla JB, Nowicki ML, et al. The clinical value of MRI using single-shot echoplanar DWI to identify liver involvement in patients with advanced gastroenteropancreatic-neuroendocrine tumors (GEP-NETs), compared to FSE T2 and FFE T1 weighted image after i.v. Gd-EOB-DTPA contrast enhancement. Med Sci Monit 2012;18:MT33–MT40.
11. Kim YK, Park G, Kim CS, Yu HC, Han YM. Diagnostic efficacy of gadoxetic acid-enhanced MRI for the detection and characterisation of liver metastases: comparison with multidetector-row CT. Br J Radiol 2012;85:539–547.
12. Van Beers BE, Pastor CM, Hussain HK. Primovist, eovist: what to expect? J Hepatol 2012;57:421–429.
13. Zech CJ, Herrmann KA, Reiser MF, Schoenberg SO. MR imaging in patients with suspected liver metastases: value of liver-specific contrast agent Gd-EOB-DTPA. Magn Reson Med Sci 2007;6:43–52.
14. Rufini V, Baum RP, Castaldi P, et al. Role of PET/CT in the functional imaging of endocrine pancreatic tumors. Abdom Imaging 2012;37:1004–1020.
15. Koh TS, Thng CH, Lee PS, et al. Hepatic metastases: in vivo assessment of perfusion parameters at dynamic contrast-enhanced MR imaging with dual-input two-compartment tracer kinetics model. Radiology 2008;249:307–320.
16. Thng CH, Koh TS, Collins DJ, Koh DM. Perfusion magnetic resonance imaging of the liver. World J Gastroenterol 2010;16:1598–1609.
17. Sourbron S, Sommer WH, Reiser MF, Zech CJ. Combined quantification of liver perfusion and function with dynamic gadoxetic acid-enhanced MR imaging. Radiology 2012;263:874–883.
18. Materne R, Smith AM, Peeters F, et al. Assessment of hepatic perfusion parameters with dynamic MRI. Magn Reson Med 2002;47: 135–142.
19. Ryeom HK, Kim SH, Kim JY, et al. Quantitative evaluation of liver function with MRI Using Gd-EOB-DTPA. Korean J Radiol 2004;5: 231–239.
20. Oberg K, Knigge U, Kwekkeboom D, Perren A. Neuroendocrine gastro-entero-pancreatic tumors: ESMO Clinical Practice Guidelines for diagnosis, treatment and follow-up. Ann Oncol 2012; 23(Suppl 7):vii124–130.
21. Binderup T, Knigge U, Loft A, et al. Functional imaging of neuroendocrine tumors: a head-to-head comparison of somatostatin receptor scintigraphy, 123I-MIBG scintigraphy, and 18F-FDG PET. J Nucl Med 2010;51:704–712.
22. Kayani I, Conry BG, Groves AM, et al. A comparison of 68Ga-DOTATATE and 18F-FDG PET/CT in pulmonary neuroendocrine tumors. J Nucl Med 2009;50:1927–1932.
23. Ambrosini V, Tomassetti P, Castellucci P, et al. Comparison between 68Ga-DOTA-NOC and 18F-DOPA PET for the detection of gastro-entero-pancreatic and lung neuro-endocrine tumours. Eur J Nucl Med Mol Imaging 2008;35:1431–1438.
24. Breeman WA, de Jong M, de Blois E, Bernard BF, Konijnenberg M, Krenning EP. Radiolabelling DOTA-peptides with 68Ga. Eur J Nucl Med Mol Imaging 2005;32:478–485.
25. Kayani I, Bomanji JB, Groves A, et al. Functional imaging of neuroendocrine tumors with combined PET/CT using 68Ga-DOTATATE (DOTA-DPhe1,Tyr3-octreotate) and 18F-FDG. Cancer 2008;112:2447–2455.
26. Haug AR, Tiega Donfack BP, Trumm C, et al. 18F-FDG PET/CT predicts survival after radioembolization of hepatic metastases from breast cancer. J Nucl Med 2012;53:371–377.
27. Fuccio C, Musto A, Cambioli S, et al. When should F-18 FDG PET/CT be used instead of 68Ga-DOTA-peptides to investigate metastatic neuroendocrine tumors? Clin Nucl Med 2011;36: 1109–1111.
28. Sourbron S, Ingrisch M, Siefert A, Reiser M, Herrmann K. Quantification of cerebral blood flow, cerebral blood volume, and blood-brain-barrier leakage with DCE-MRI. Magn Reson Med 2009;62:205–217.
29. Makkat S, Luypaert R, Stadnik T, et al. Deconvolution-based dynamic contrast-enhanced MR imaging of breast tumors: correlation of tumor blood flow with human epidermal growth factor receptor 2 status and clinicopathologic findings-preliminary results. Radiology 2008;249:471–482.
30. Do RK, Rusinek H, Taouli B. Dynamic contrast-enhanced MR imaging of the liver: current status and future directions. Magn Reson Imaging Clin N Am 2009;17:339–349.
31. Nilsson H, Nordell A, Vargas R, Douglas L, Jonas E, Blomqvist L. Assessment of hepatic extraction fraction and input relative blood flow using dynamic hepatocyte-specific contrast-enhanced MRI. J Magn Reson Imaging 2009;29:1323–1331.
32. Giesel FL, Kratochwil C, Mehndiratta A, et al. Comparison of neuroendocrine tumor detection and characterization using DOTATOC-PET in correlation with contrast enhanced CT and delayed contrast enhanced MRI. Eur J Radiol 2012;81:2820–2825.
33. Pfannenberg C, Schraml C, Schwenzer N, et al. Comparison of [68Ga]DOTATOC-PET/CT and whole-body MRI in staging of neuroendocrine tumors. Cancer Imaging 2011;11(Spec No A):S38–S39.
34. Kamaya A, Maturen KE, Tye GA, Liu YI, Parti NN, Desser TS. Hypervascular liver lesions. Semin Ultrasound CT MR 2009;30: 387–407.
35. Scoazec JY. Angiogenesis in neuroendocrine tumors: therapeutic applications. Neuroendocrinology 2013;97:45–56.

36. Weinmann HJ, Bauer H, Frenzel T, Muhler A, Ebert W. Mechanism of hepatic uptake of gadoxetate disodium. Acad Radiol 1996;(Suppl 2):S232–S234.
37. Miyazaki K, Orton MR, Davidson RL, et al. Neuroendocrine tumor liver metastases: use of dynamic contrast-enhanced MR imaging to monitor and predict radiolabeled octreotide therapy response. Radiology 2012;263:139–148.
38. Soret M, Bacharach SL, Buvat I. Partial-volume effect in PET tumor imaging. J Nucl Med 2007;48:932–945.
39. Schreiter NF, Nogami M, Steffen I, et al. Evaluation of the potential of PET-MRI fusion for detection of liver metastases in patients with neuroendocrine tumours. Eur Radiol 2012;22:458–467.
40. Huppertz A, Haraida S, Kraus A, et al. Enhancement of focal liver lesions at gadoxetic acid-enhanced MR imaging: correlation with histopathologic findings and spiral CT-initial observations. Radiology 2005;234:468–478.

7. Literaturverzeichnis

1. Sourbron S, Sommer WH, Reiser MF, Zech CJ. Combined quantification of liver perfusion and function with dynamic gadoxetic acid-enhanced MR imaging. *Radiology* 2012; **263**(3): 874-83.
2. Auernhammer CJ, Goke B. Therapeutic strategies for advanced neuroendocrine carcinomas of jejunum/ileum and pancreatic origin. *Gut* 2011; **60**(7): 1009-21.
3. Niederle B, Pape UF, Costa F, et al. ENETS Consensus Guidelines Update for Neuroendocrine Neoplasms of the Jejunum and Ileum. *Neuroendocrinology* 2016; **103**(2): 125-38.
4. Yao JC, Hassan M, Phan A, et al. One hundred years after "carcinoid": epidemiology of and prognostic factors for neuroendocrine tumors in 35,825 cases in the United States. *J Clin Oncol* 2008; **26**(18): 3063-72.
5. Sahu S, Schernthaner R, Ardon R, et al. Imaging Biomarkers of Tumor Response in Neuroendocrine Liver Metastases Treated with Transarterial Chemoembolization: Can Enhancing Tumor Burden of the Whole Liver Help Predict Patient Survival? *Radiology* 2017; **283**(3): 883-94.
6. Bashir U, Mallia A, Stirling J, et al. PET/MRI in Oncological Imaging: State of the Art. *Diagnostics (Basel)* 2015; **5**(3): 333-57.
7. Singnurkar A, Poon R, Metser U. Comparison of 18F-FDG-PET/CT and 18F-FDG-PET/MR imaging in oncology: a systematic review. *Ann Nucl Med* 2017; **31**(5): 366-78.
8. Koh TS, Thng CH, Hartono S, et al. Dynamic contrast-enhanced MRI of neuroendocrine hepatic metastases: A feasibility study using a dual-input two-compartment model. *Magn Reson Med* 2011; **65**(1): 250-60.
9. Miyazaki K, Orton MR, Davidson RL, et al. Neuroendocrine tumor liver metastases: use of dynamic contrast-enhanced MR imaging to monitor and predict radiolabeled octreotide therapy response. *Radiology* 2012; **263**(1): 139-48.
10. Weiss J, Ruff C, Grosse U, et al. Assessment of Hepatic Perfusion Using GRASP MRI: Bringing Liver MRI on a New Level. *Invest Radiol* 2019; **54**(12): 737-43.
11. Ramage JK, Ahmed A, Ardill J, et al. Guidelines for the management of gastroenteropancreatic neuroendocrine (including carcinoid) tumours (NETs). *Gut* 2012; **61**(1): 6-32.
12. Chai SM, Brown IS, Kumarasinghe MP. Gastroenteropancreatic neuroendocrine neoplasms: selected pathology review and molecular updates. *Histopathology* 2018; **72**(1): 153-67.
13. Kim JY, Hong SM, Ro JY. Recent updates on grading and classification of neuroendocrine tumors. *Ann Diagn Pathol* 2017; **29**: 11-6.
14. Granata V, Fusco R, Setola SV, et al. The multidisciplinary team for gastroenteropancreatic neuroendocrine tumours: the radiologist's challenge. *Radiol Oncol* 2019; **53**(4): 373-87.
15. Kim KW, Krajewski KM, Nishino M, et al. Update on the management of gastroenteropancreatic neuroendocrine tumors with emphasis on the role of imaging. *AJR Am J Roentgenol* 2013; **201**(4): 811-24.
16. Mohamed A, Strosberg JR. Medical Management of Gastroenteropancreatic Neuroendocrine Tumors: Current Strategies and Future Advances. *J Nucl Med* 2019; **60**(6): 721-7.
17. Deroose CM, Hindie E, Kebebew E, et al. Molecular Imaging of Gastroenteropancreatic Neuroendocrine Tumors: Current Status and Future Directions. *J Nucl Med* 2016; **57**(12): 1949-56.
18. Rufini V, Baum RP, Castaldi P, et al. Role of PET/CT in the functional imaging of endocrine pancreatic tumors. *Abdom Imaging* 2012; **37**(6): 1004-20.
19. Weber W. Clinical PET/MR. *Recent Results Cancer Res* 2020; **216**: 747-64.
20. Sundin A, Arnold R, Baudin E, et al. ENETS Consensus Guidelines for the Standards of Care in Neuroendocrine Tumors: Radiological, Nuclear Medicine & Hybrid Imaging. *Neuroendocrinology* 2017; **105**(3): 212-44.
21. Debray MP, Geoffroy O, Laissy JP, et al. Imaging appearances of metastases from neuroendocrine tumours of the pancreas. *Br J Radiol* 2001; **74**(887): 1065-70.
22. Ronot M, Clift AK, Baum RP, et al. Morphological and Functional Imaging for Detecting and Assessing the Resectability of Neuroendocrine Liver Metastases. *Neuroendocrinology* 2018; **106**(1): 74-88.

23. Morin C, Drolet S, Daigle C, et al. Additional value of gadoxetic acid-enhanced MRI to conventional extracellular gadolinium-enhanced MRI for the surgical management of colorectal and neuroendocrine liver metastases. *HPB (Oxford)* 2020; **22**(5): 710-5.
24. Vilgrain V, Esvan M, Ronot M, Caumont-Prim A, Aube C, Chatellier G. A meta-analysis of diffusion-weighted and gadoxetic acid-enhanced MR imaging for the detection of liver metastases. *Eur Radiol* 2016; **26**(12): 4595-615.
25. Zech CJ, Herrmann KA, Reiser MF, Schoenberg SO. MR imaging in patients with suspected liver metastases: value of liver-specific contrast agent Gd-EOB-DTPA. *Magn Reson Med Sci* 2007; **6**(1): 43-52.
26. Armbruster M, Sourbron S, Haug A, et al. Evaluation of neuroendocrine liver metastases: a comparison of dynamic contrast-enhanced magnetic resonance imaging and positron emission tomography/computed tomography. *Invest Radiol* 2014; **49**(1): 7-14.
27. Armbruster M, Zech CJ, Sourbron S, et al. Diagnostic accuracy of dynamic gadoxetic-acid-enhanced MRI and PET/CT compared in patients with liver metastases from neuroendocrine neoplasms. *J Magn Reson Imaging* 2014; **40**(2): 457-66.

Danksagung

Ich möchte mich hiermit bei Herrn Prof. Dr. med. Jens Ricke, Direktor der Klinik und Poliklinik für Radiologie des LMU Klinikum sowie dessen Vorgänger Prof. Dr. med. Dr. h.c. Maximilian Reiser, bedanken, die mir die Möglichkeit gegeben haben, diese Arbeit an Ihrer Klinik durchzuführen.

Herrn Prof. Dr. med. Wieland Sommer, MPH, sowie Herrn Prof. Dr. Christoph Zech gilt ein ganz besonderer Dank, für die hervorragende Betreuung, Begeisterungsfähigkeit sowie ständige Diskussions- und Hilfsbereitschaft.

Danken möchte ich darüber hinaus allen Koautoren der Studien, deren wertvollen Anregungen und Hilfsbereitschaft wesentlich zum Gelingen dieser Arbeit beigetragen haben.

Bei meiner Ehefrau sowie meinen Eltern möchte ich mich besonders herzlich bedanken für die uneingeschränkte, liebevolle und vielseitige Unterstützung während meines Studiums und der Promotion.